The Structure and Thickness of Europa's Ice Shell

What we think we know, and what we hope to learn from the Europa Clipper

Louise Prockter

Lunar and Planetary Science Institute

Accessing the Subsurface of Ocean Worlds
October 9 2017

LPI

Interior ocean

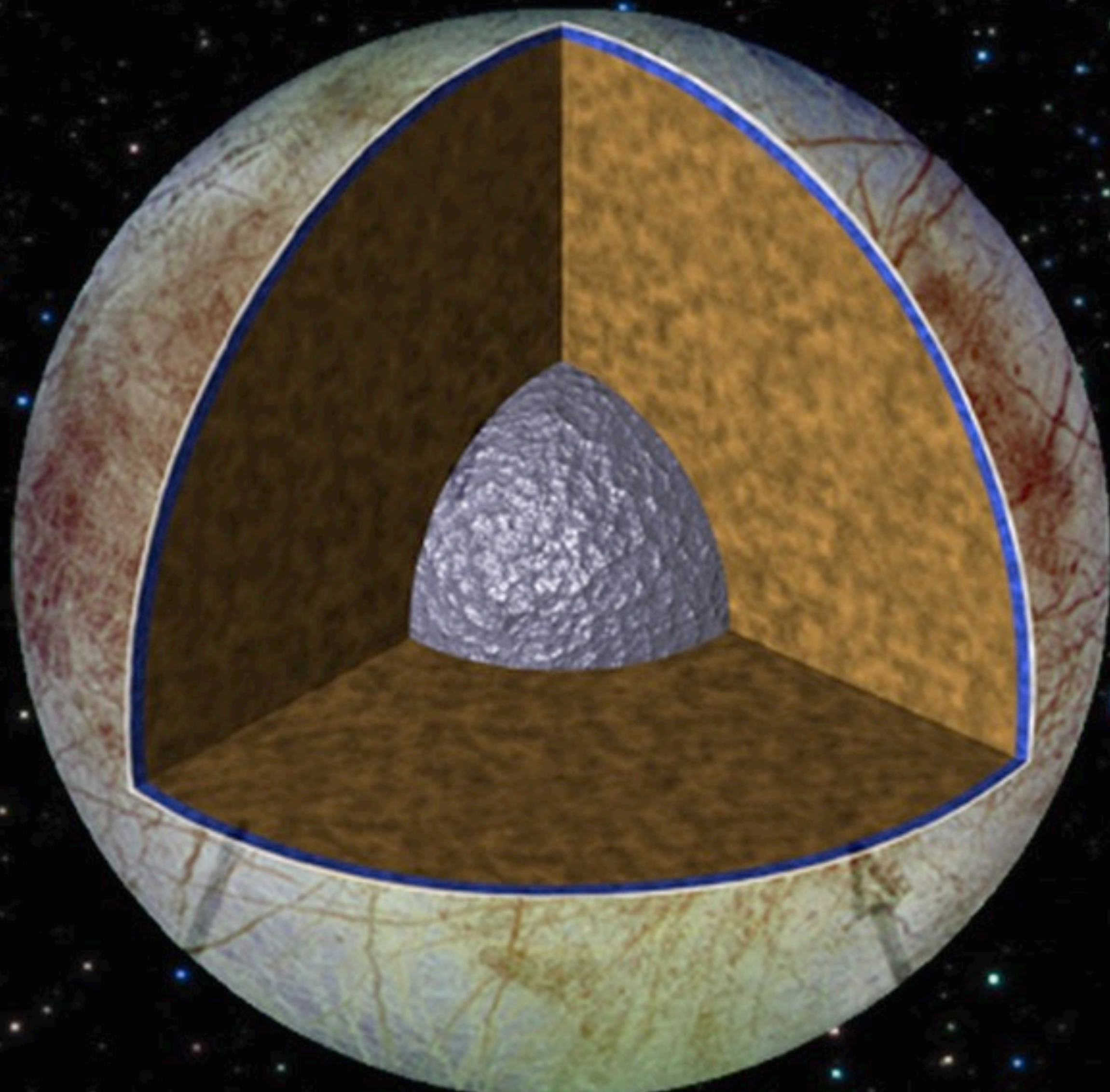

The thickness of Europa's ice shell has been the subject of intense debate – estimates range from a few km to ~30 km

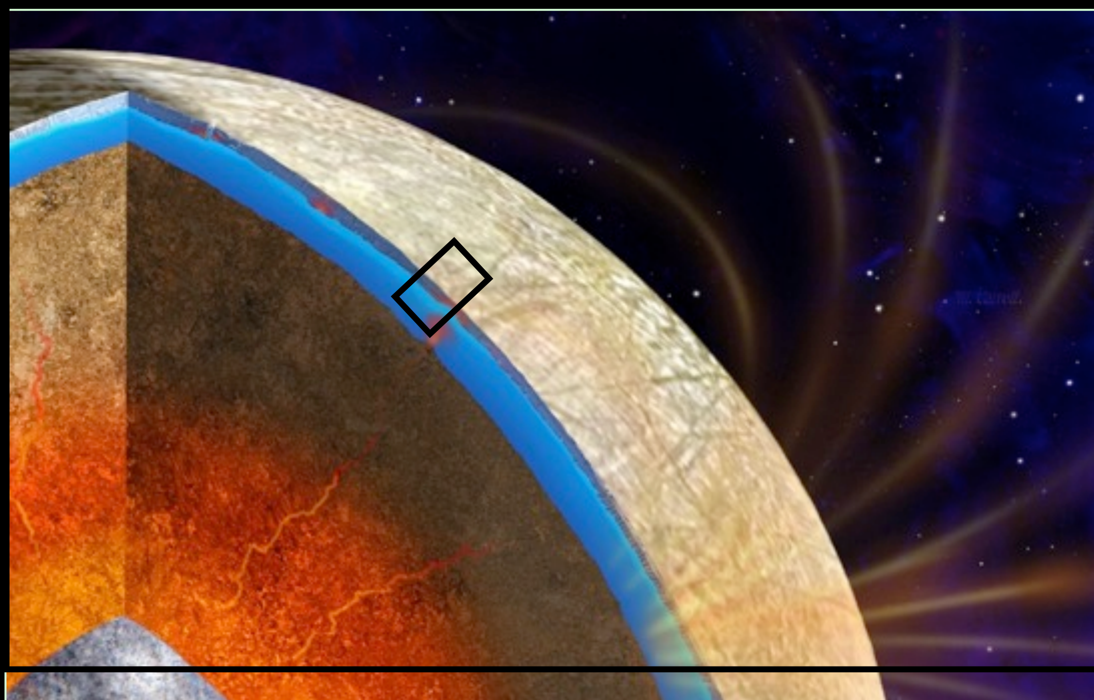

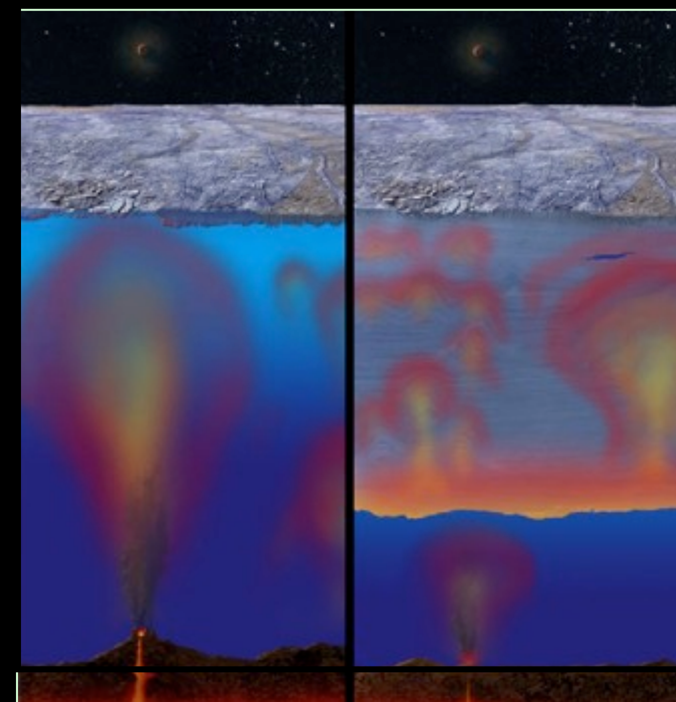

Temperature structure

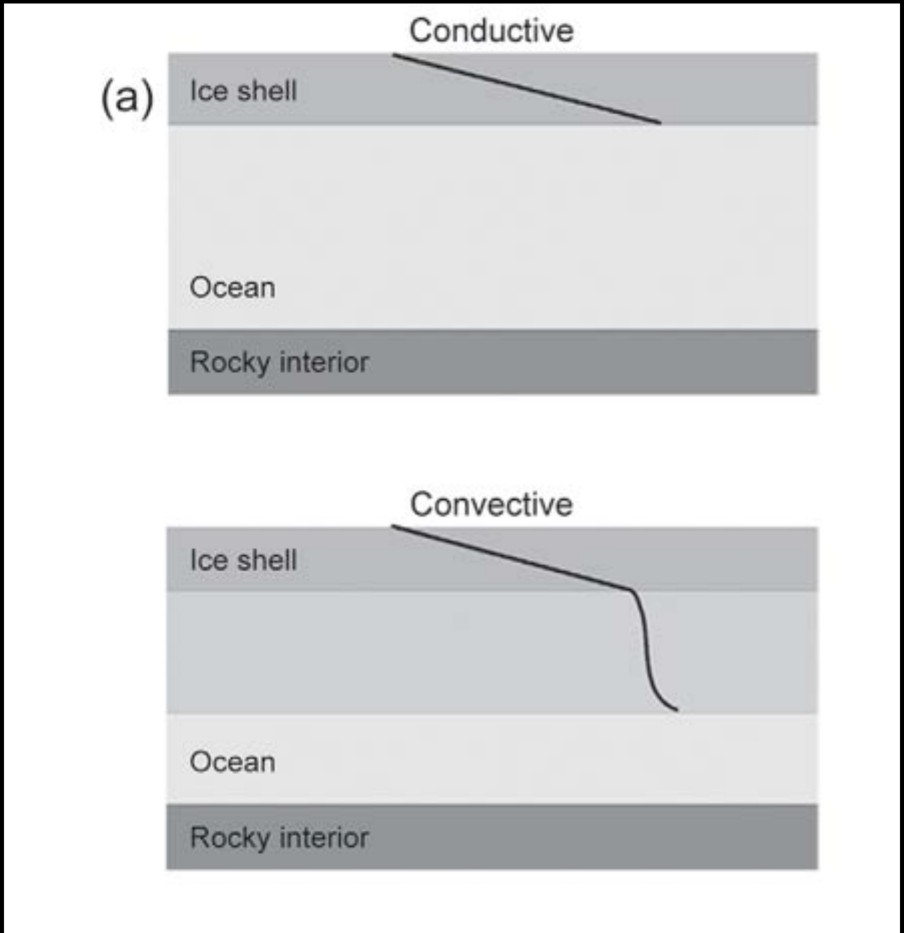

Mitri and Showman, 2005

Galileo coverage of Europa

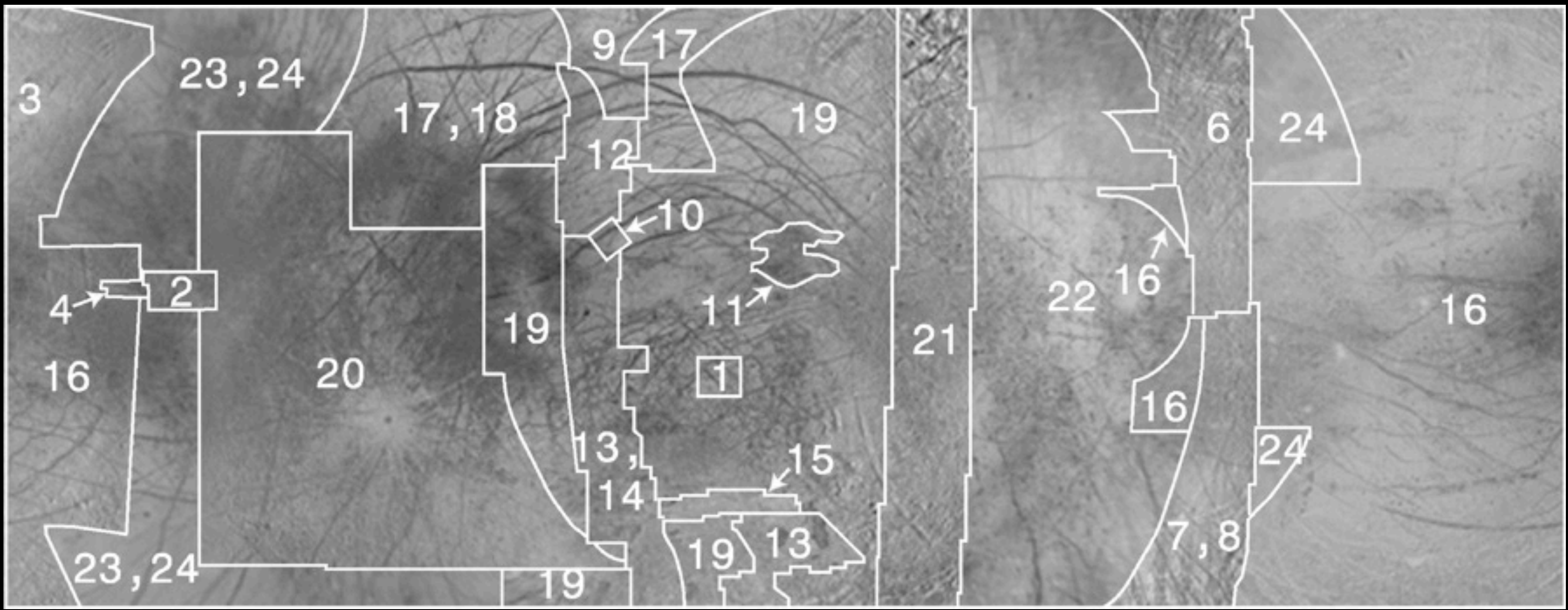

Resolution (km/pixel)	Very High (0-0.1)	Regional (0.1-0.5)	Large-scale (0.5-1)	Global (1-20)
Europa	< 0.5%	13.5%	24.5%	60.8%

Europa’s surface shows evidence for two major styles of deformation

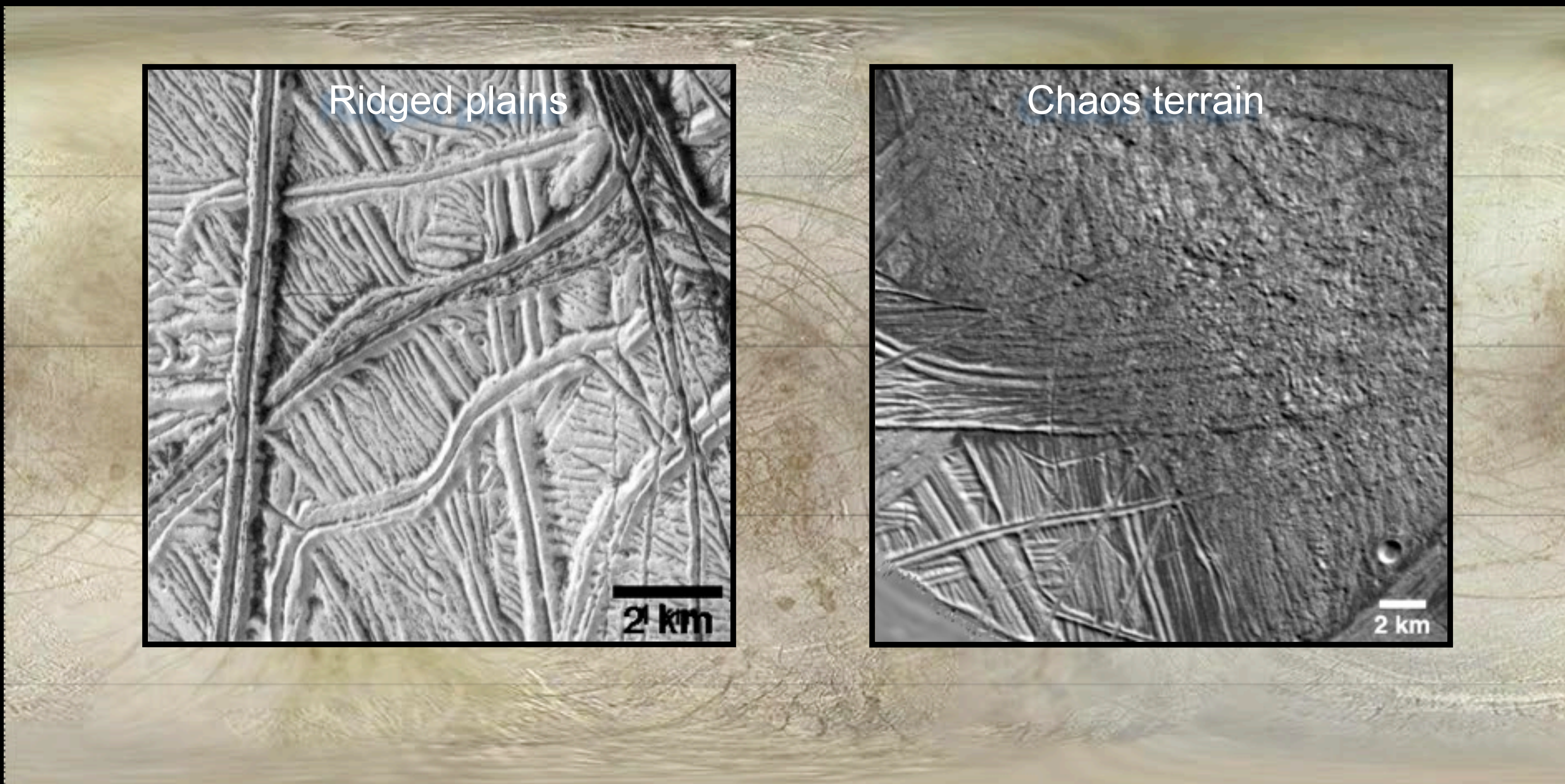

Europa’s eccentric orbit

- For an eccentric satellite orbit, permanent bulge faces empty focus
- Radial tide of ~30 m for Europa if ice shell is decoupled by ocean
- Tidal bulge librates to face Jupiter’s center of mass
- Tidal deformation dissipates energy ⇒ tidal heating
- Misaligned tidal bulge and ice thickness variations promote nonsynchronous rotation

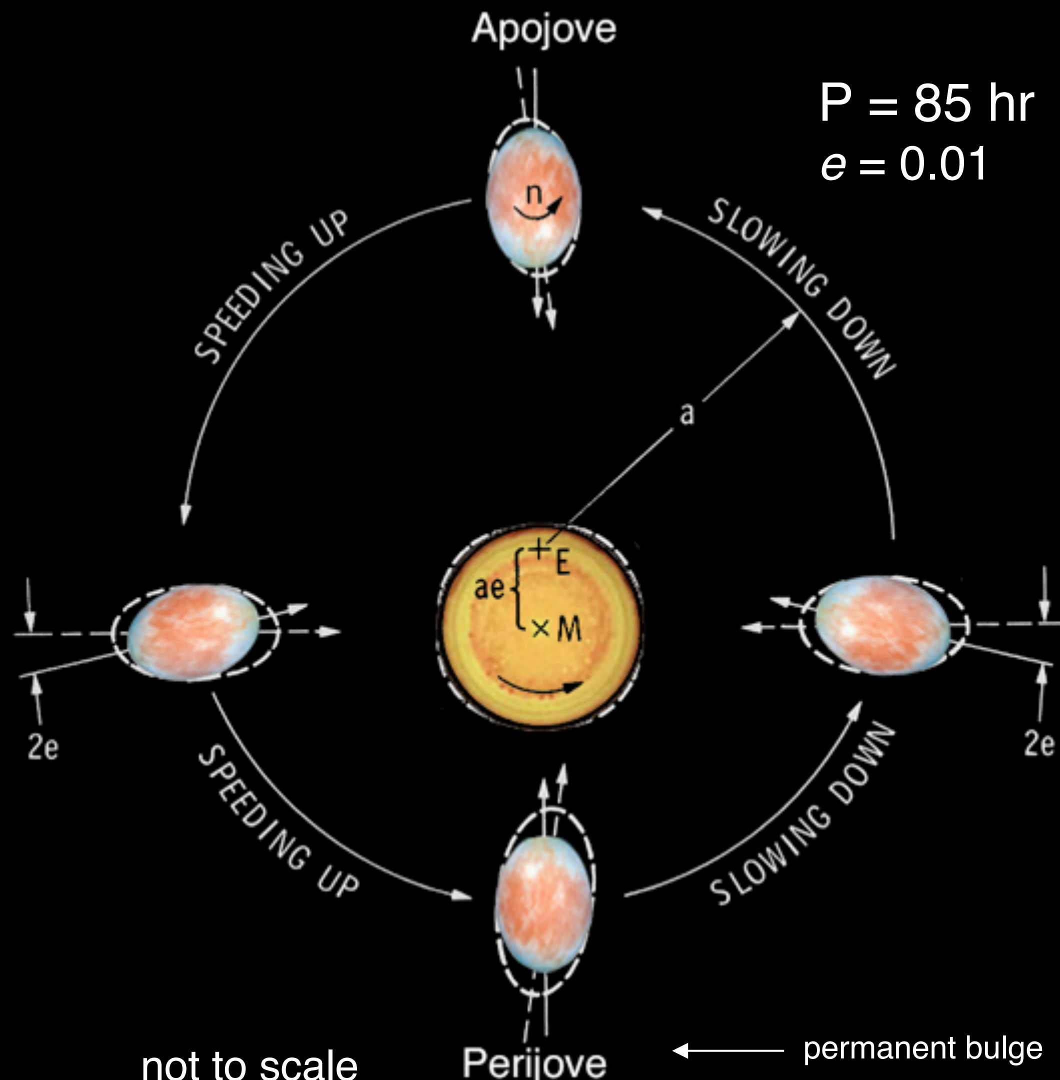

[after *Nash et al., 1982*]

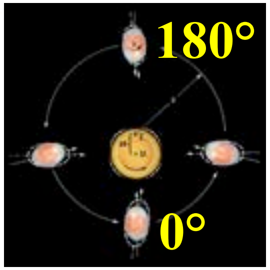

Diurnal stresses

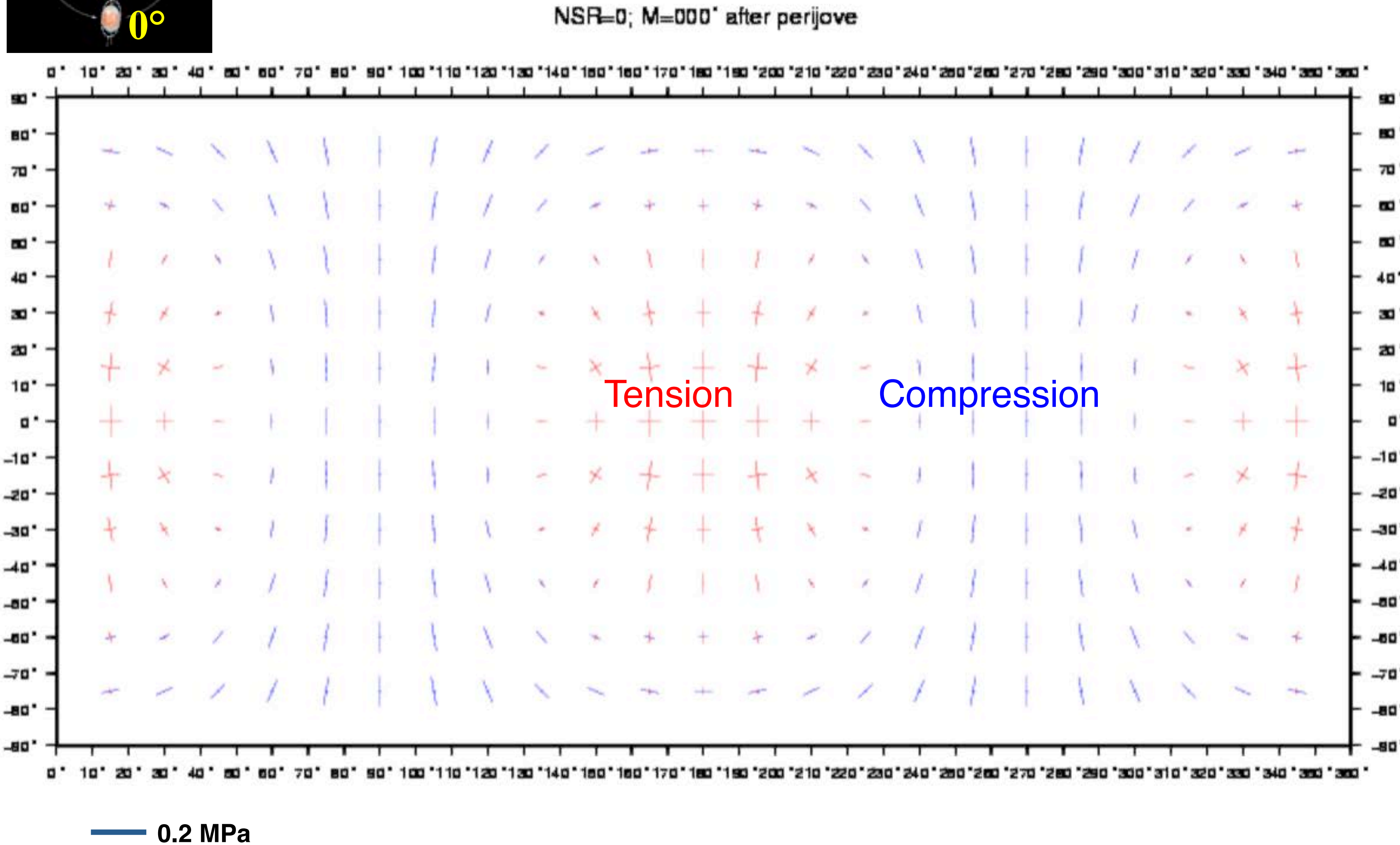

Non-synchronous rotation

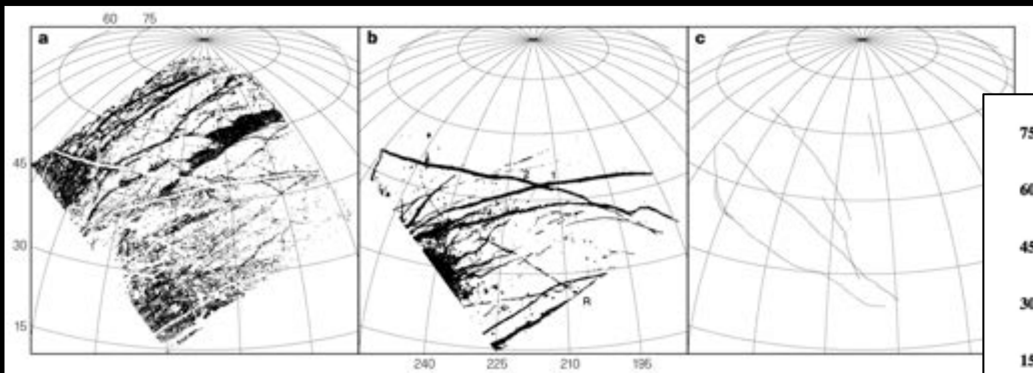

Geissler et al. (1998)

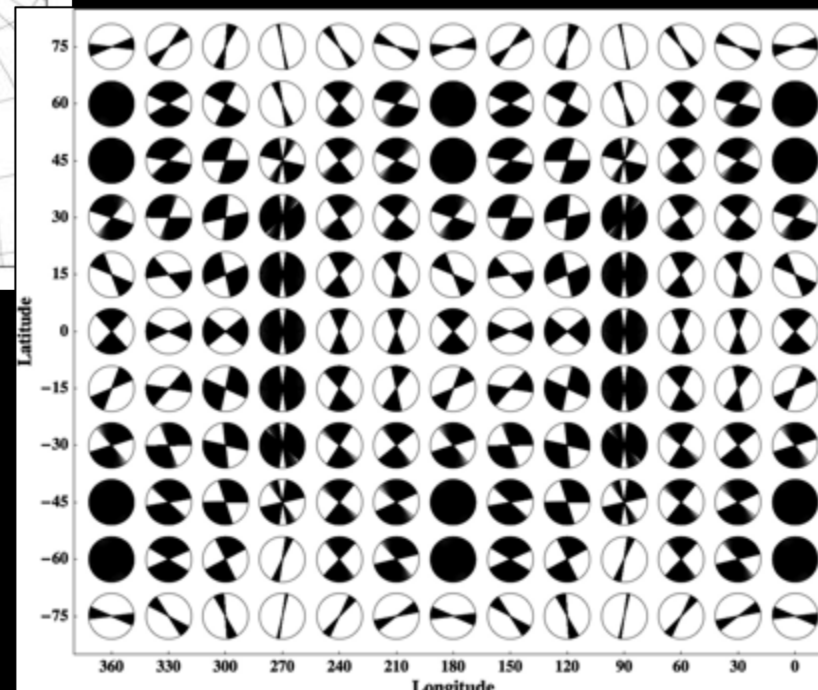

Rhoden and Hurford (2013)

Analysis of the orientation and distribution of surface lineaments and correlation to past stress fields by Geissler et al. (1998) suggests that Europa spins faster than the synchronous rate, or did so in the past

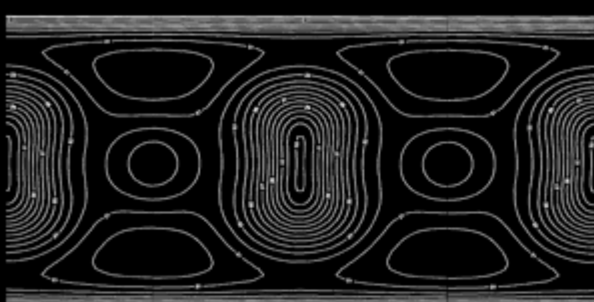

[*Ojakangas & Stevenson, 1989*]

However, analysis of lineament azimuths in Europa's Bright Plains region by Rhoden and Hurford (2013) suggests ~1º of forced obliquity and little support for non-synchronous rotation

Ridges

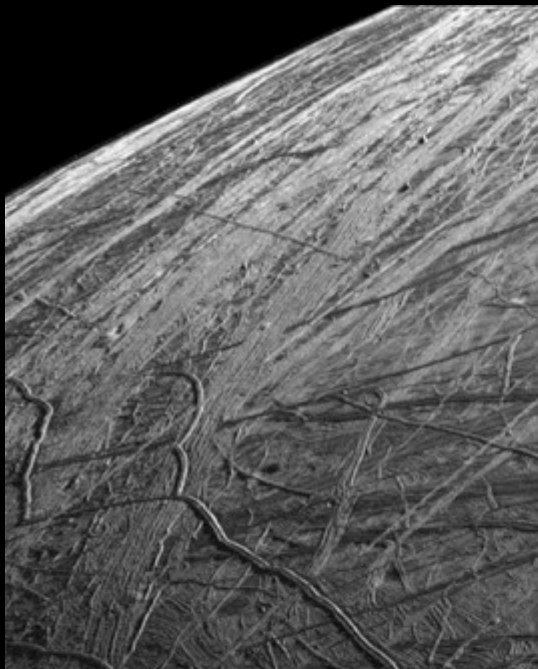

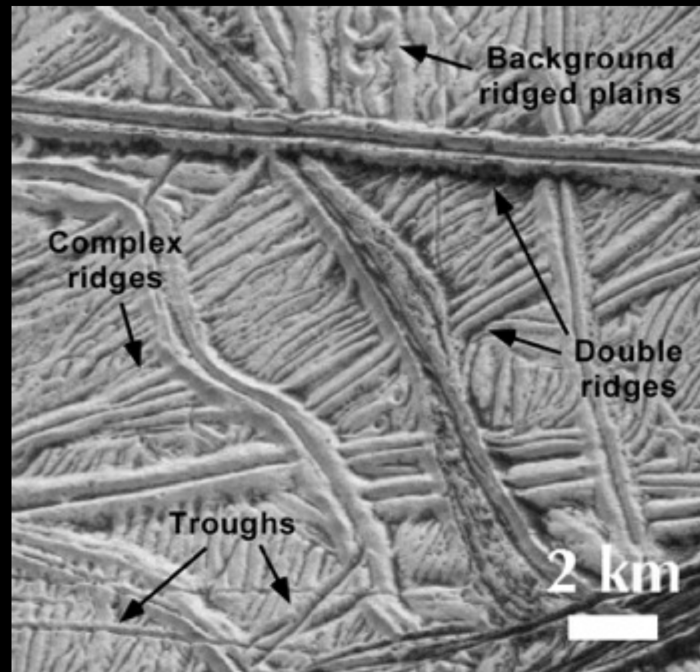
Background ridged plains
Complex ridges
Double ridges
Troughs
2 km

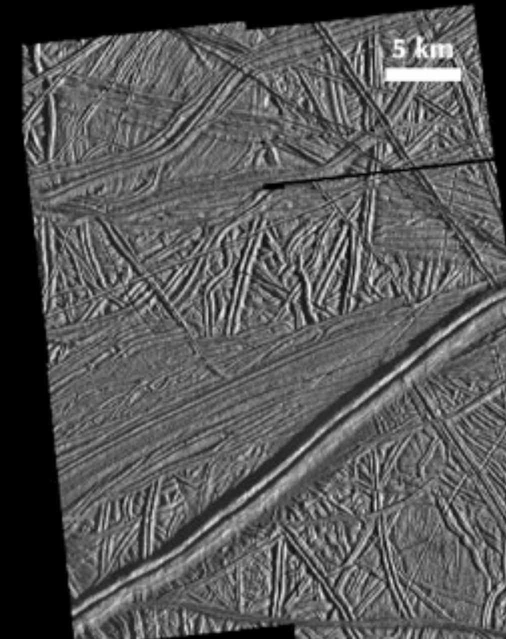
5 km

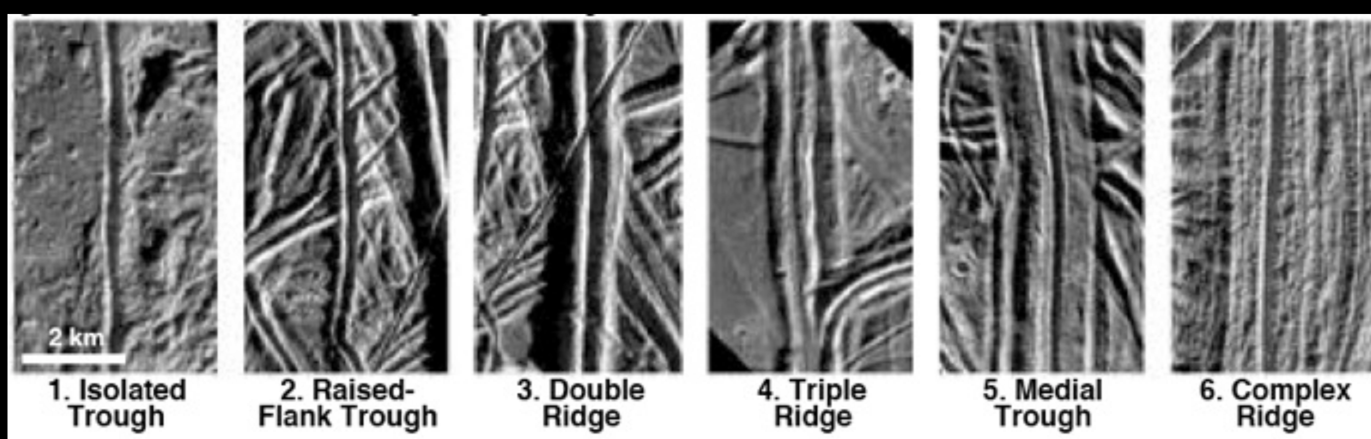
2 km
1. Isolated Trough
2. Raised-Flank Trough
3. Double Ridge
4. Triple Ridge
5. Medial Trough
6. Complex Ridge

Ridge formation models

- Double ridges: extrusion or intrusion of water or warm ice
- Shear heating from strike-slip motion along fractures could warm and melt ice
- Ridge origin models have different implications for ocean communication

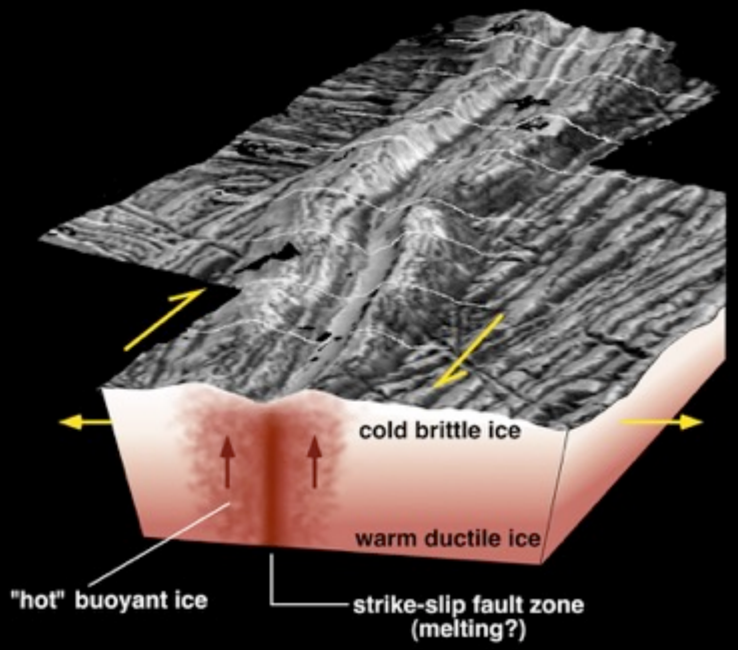

Nimmo and Gaidos, 2002

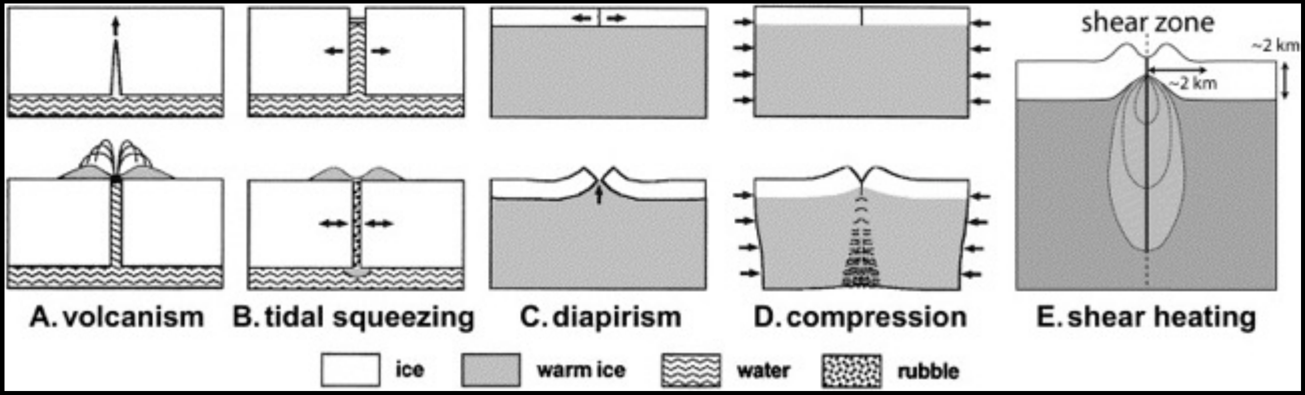

Greenberg et al., 1998; Pappalardo et al., 1998

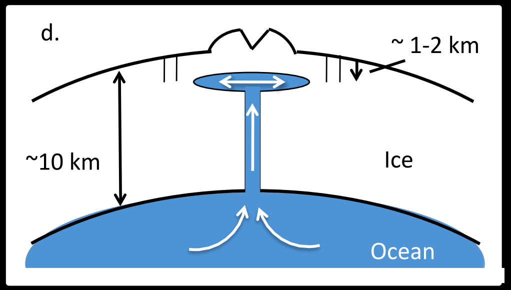

Craft et al., 2016

Cycloidal Fractures

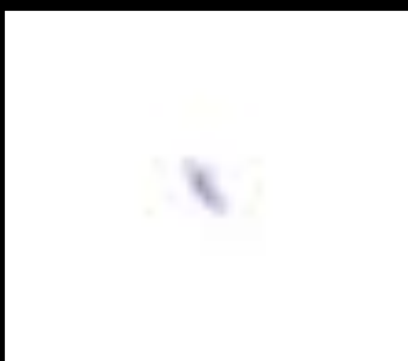

rotating diurnal stresses

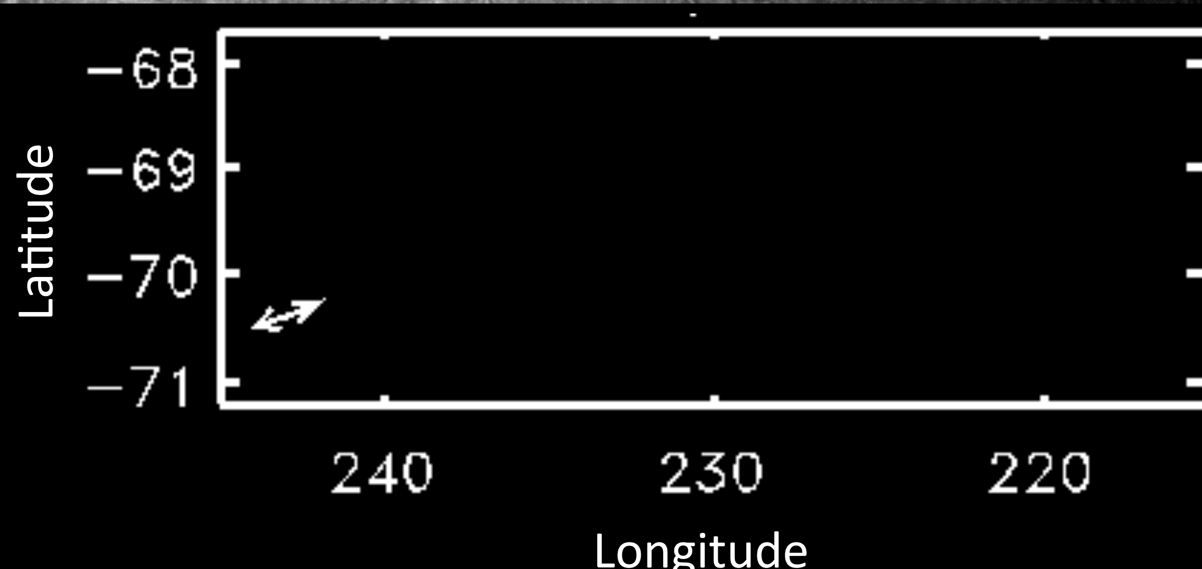

[*Hoppa et al., 1999*]

- Cycloidal fractures are explained by time-varying diurnal stresses
- Ocean is necessary for sufficient tidal amplitude and stress

Small-Circle Depressions
AKA Crop circles

Broad arcuate regional-scale troughs and depressions on Europa do not fit current diurnal or proposed NSR stresses (Schenk et al., 2008)

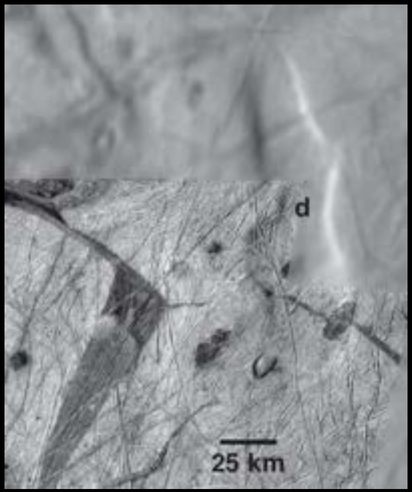

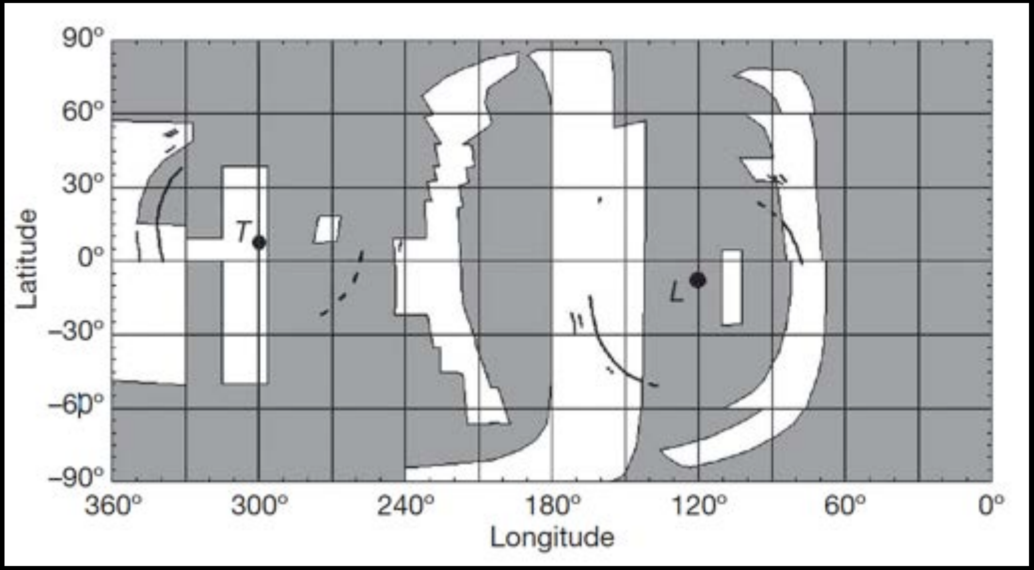

Schenk et al., 2008

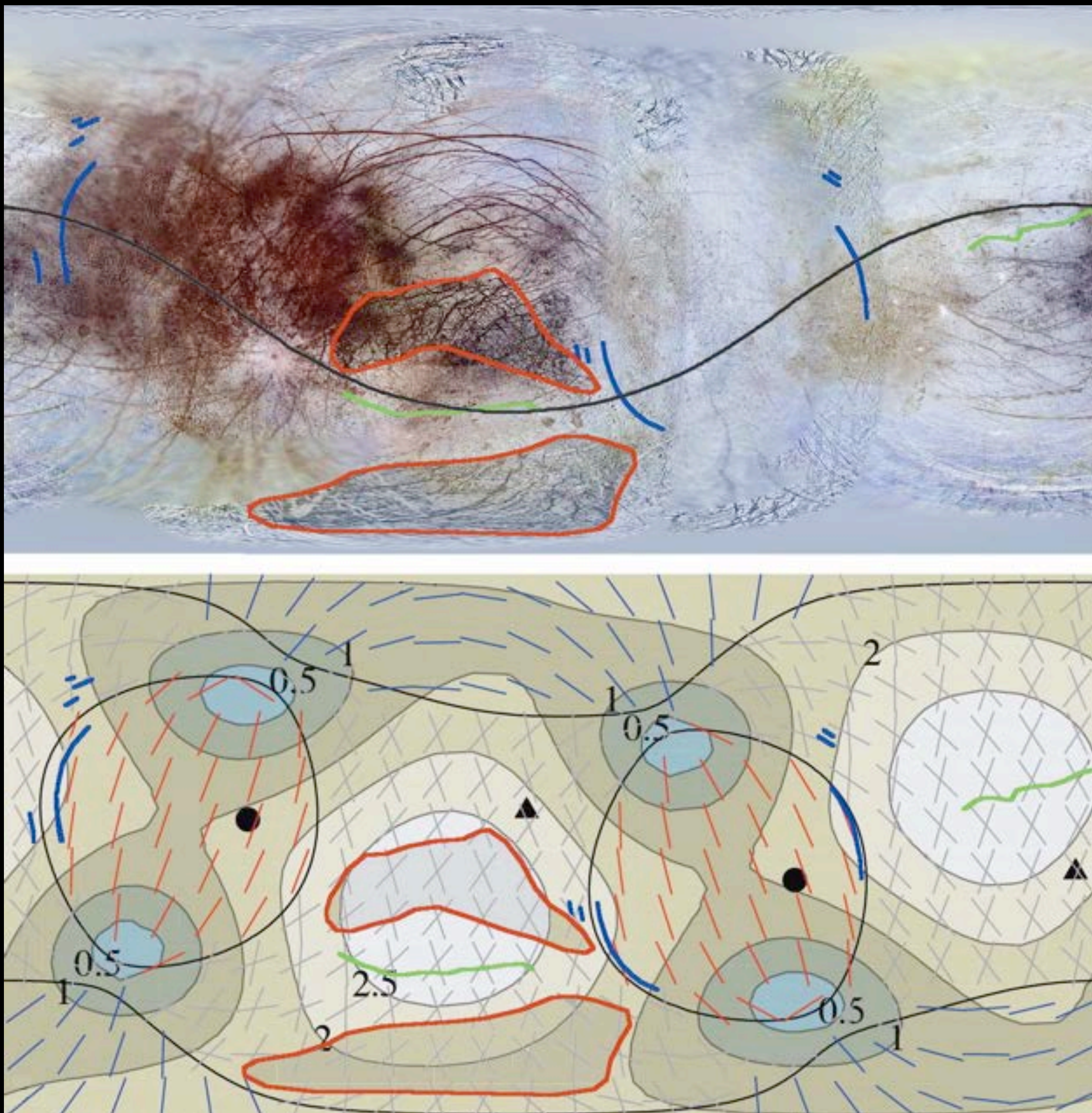

Troughs can be matched with stresses predicted by an episode of 80º of true polar wander

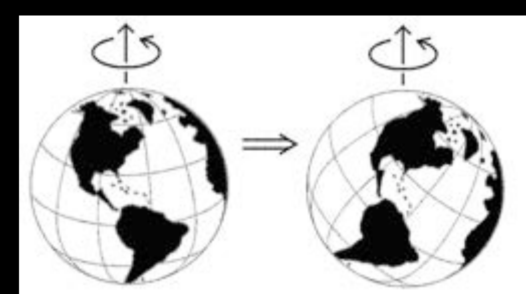

Schenk et al., 2008

Pull-apart bands: Evidence of a mobile lithosphere

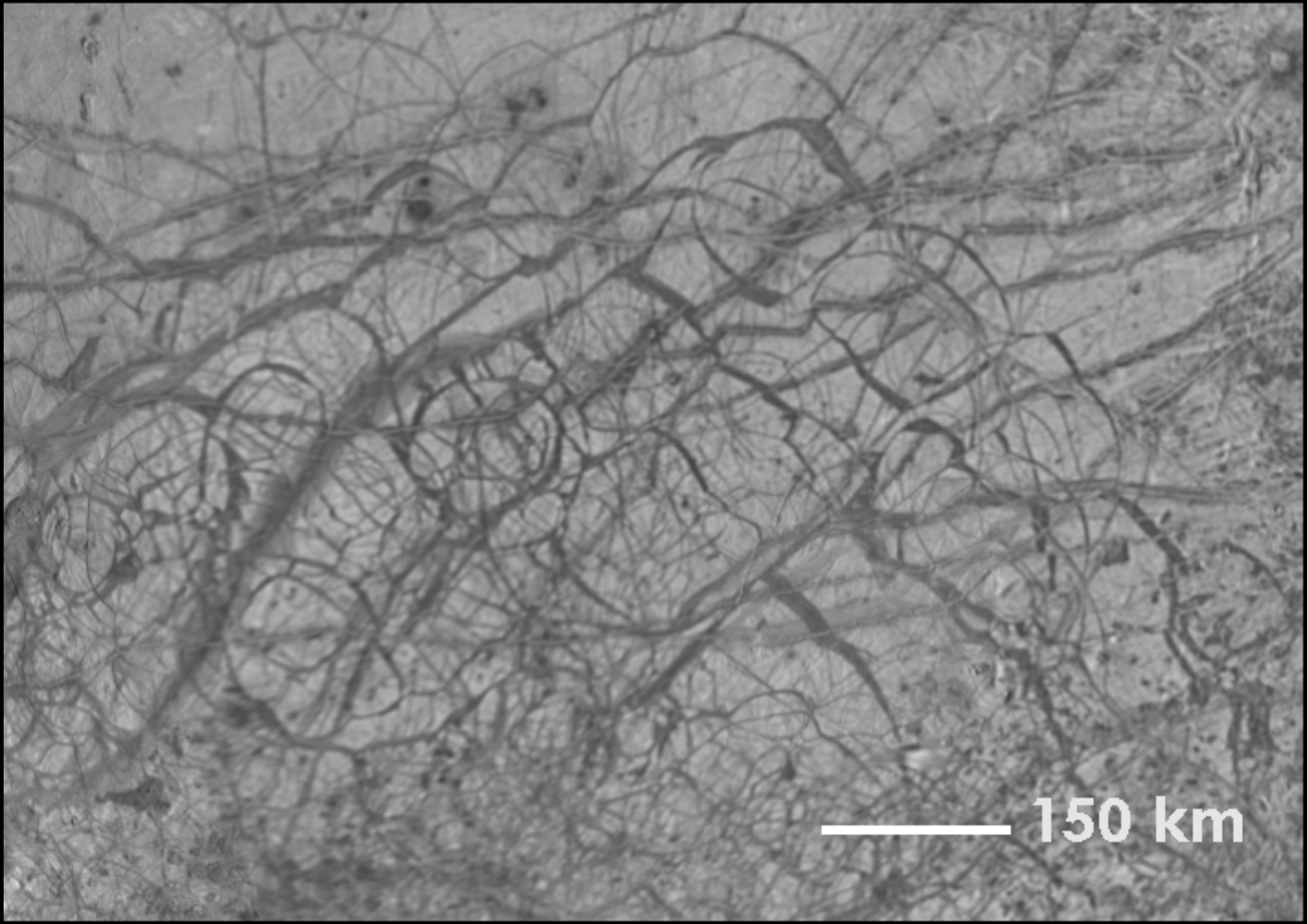

anti-jovian

Pull-apart bands

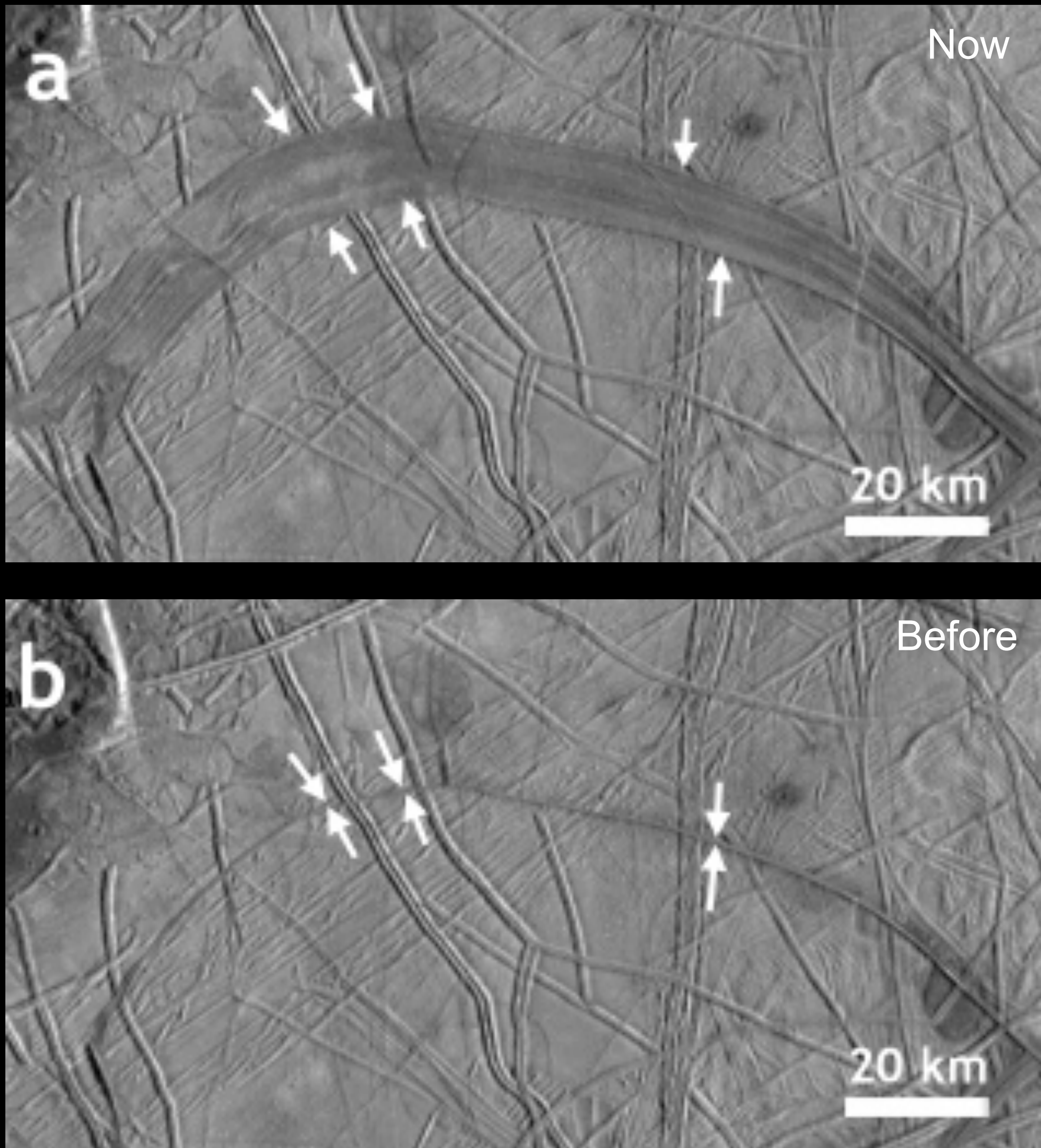

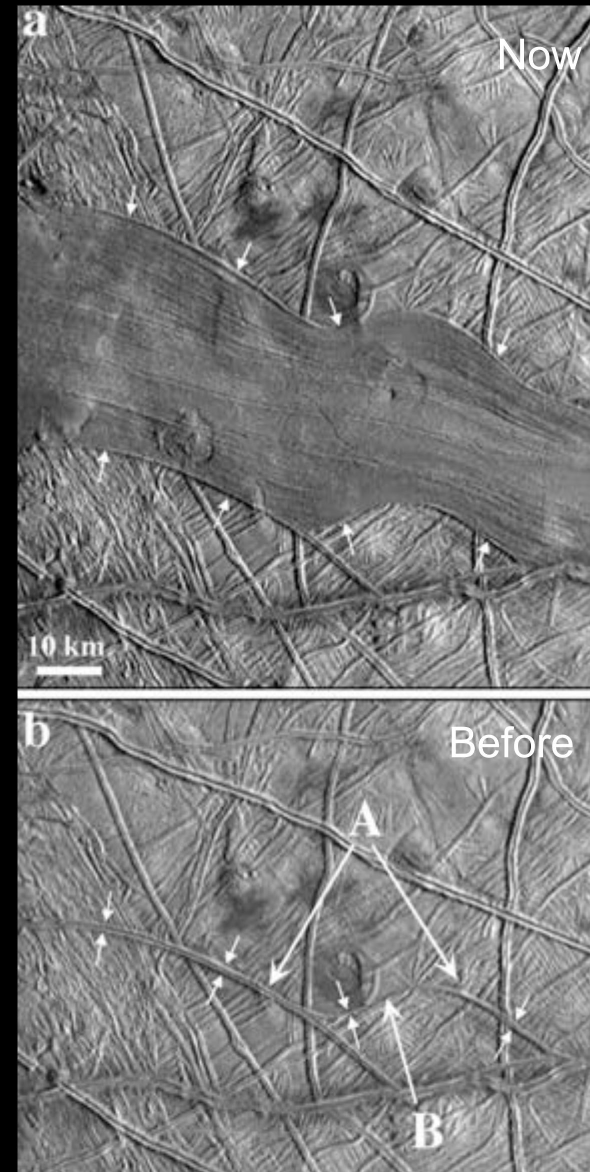

High-standing topography, bilateral symmetry, and similarities in interior morphologies suggest a similar formation mechanism to terrestrial mid-ocean ridges, with band morphology a function of spreading rate

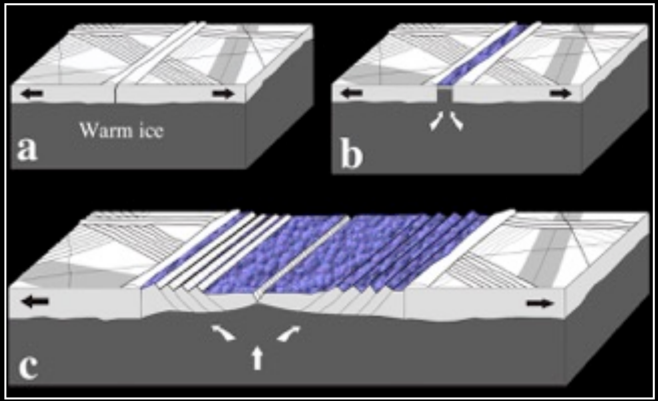

Prockter et al., 2002

New modeling by Howell and Pappalardo (2017) suggests that differences in band morphology may be a function of lithospheric strength at the time of formation

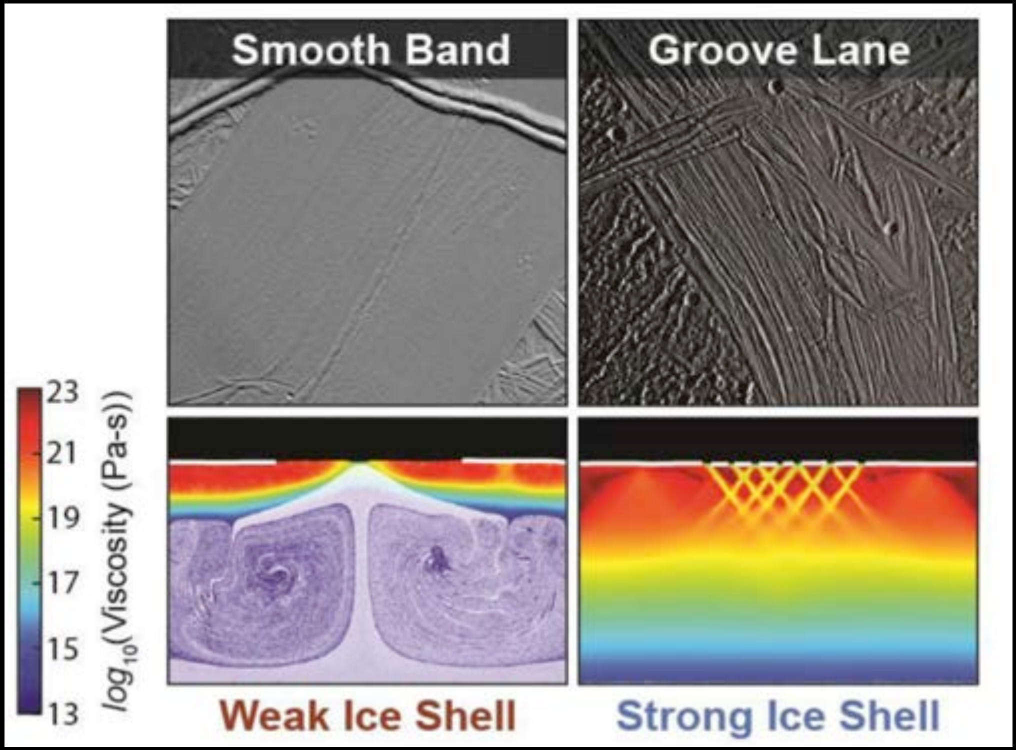

Howell and Pappalardo, 2017

Accommodation of extension may be via subduction

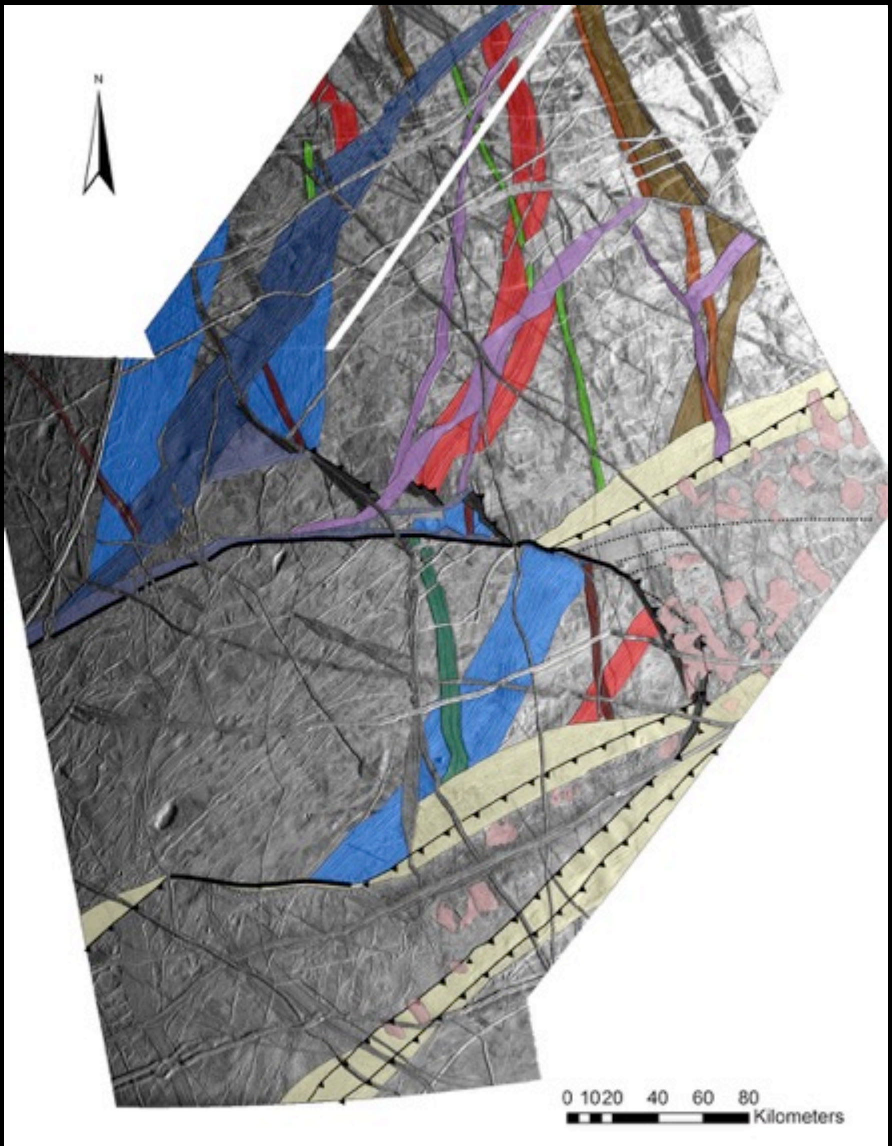

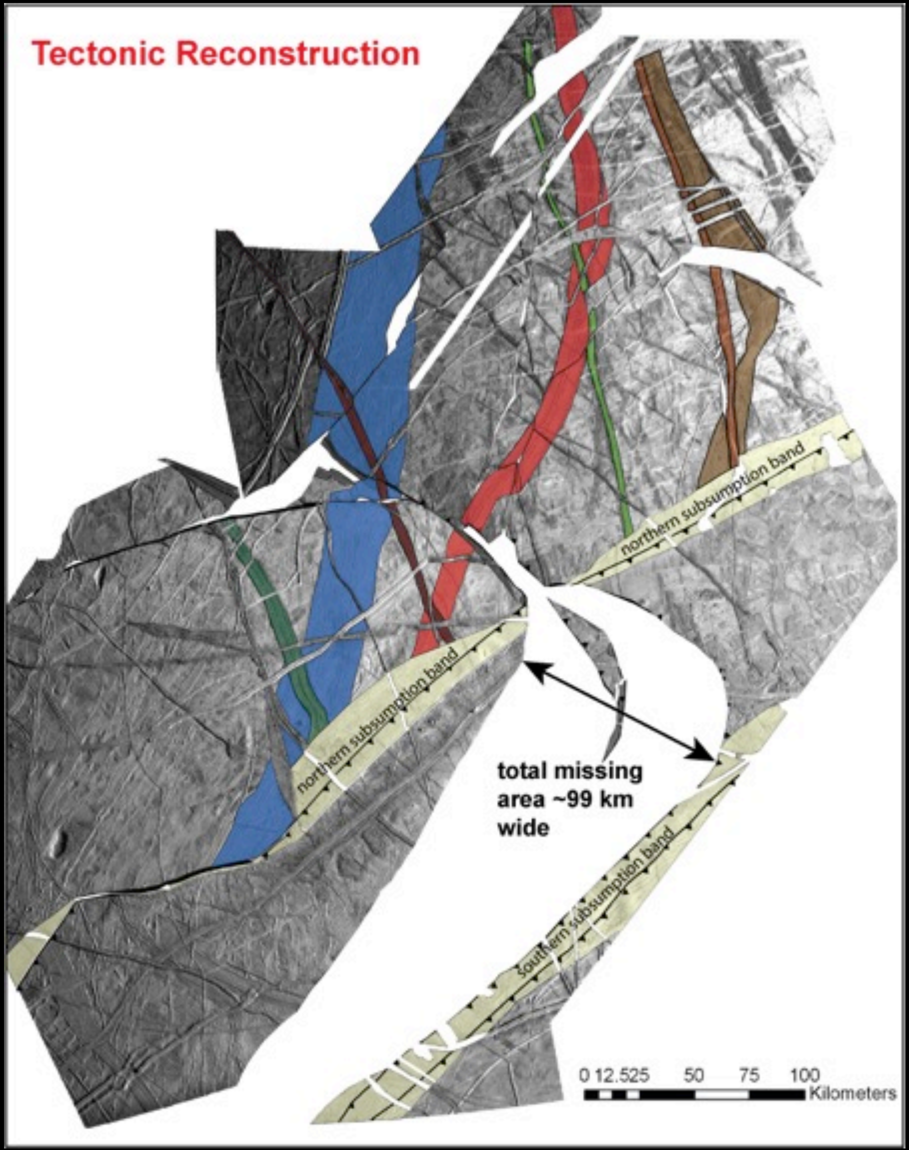

Kattenhorn and Prockter, 2014

Subduction model

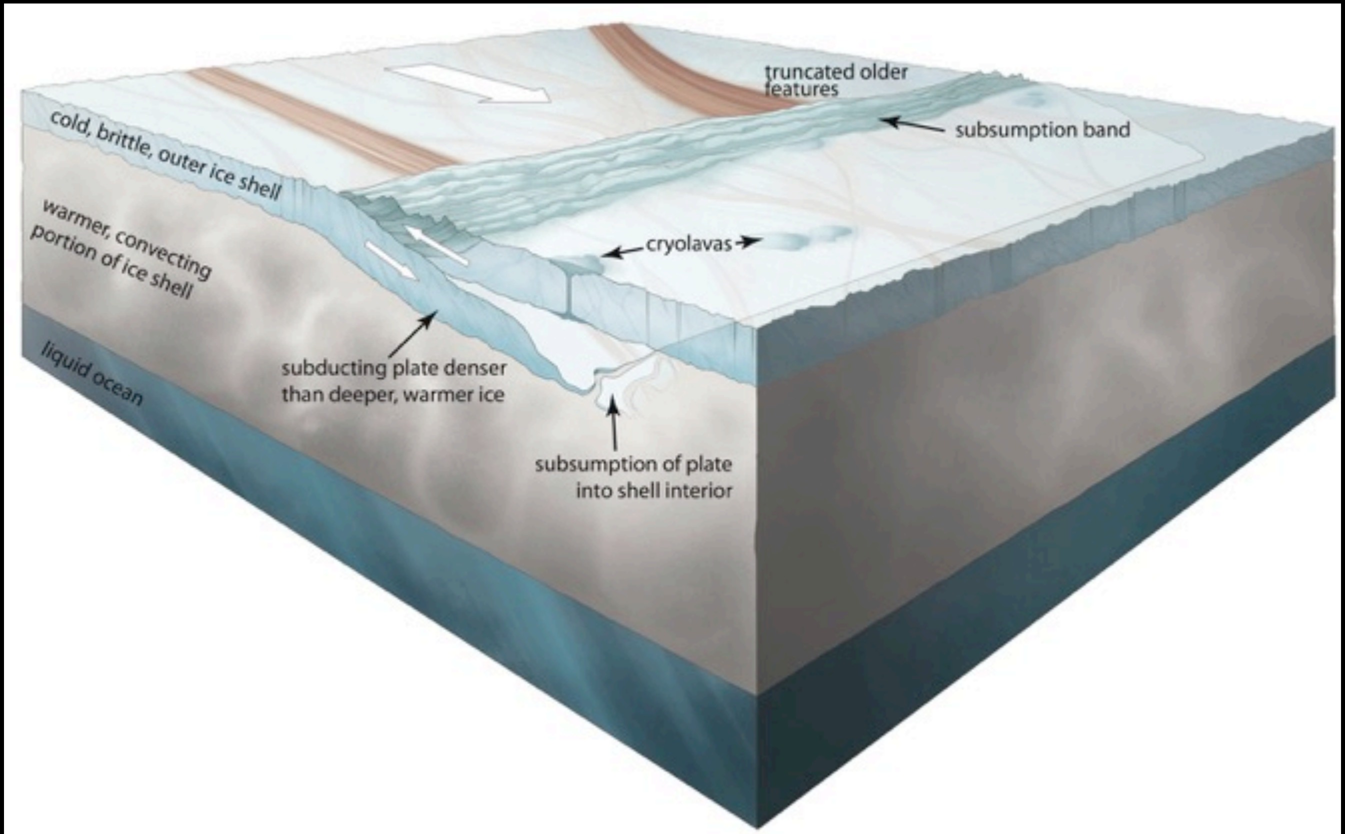

Kattenhorn and Prockter, 2014

Plates would be subsumed below the brittle ice layer (few km) into the warmer subsurface portion of the ice shell

Castalia Macula

Low-albedo depression between two significantly disrupted uplifted domes

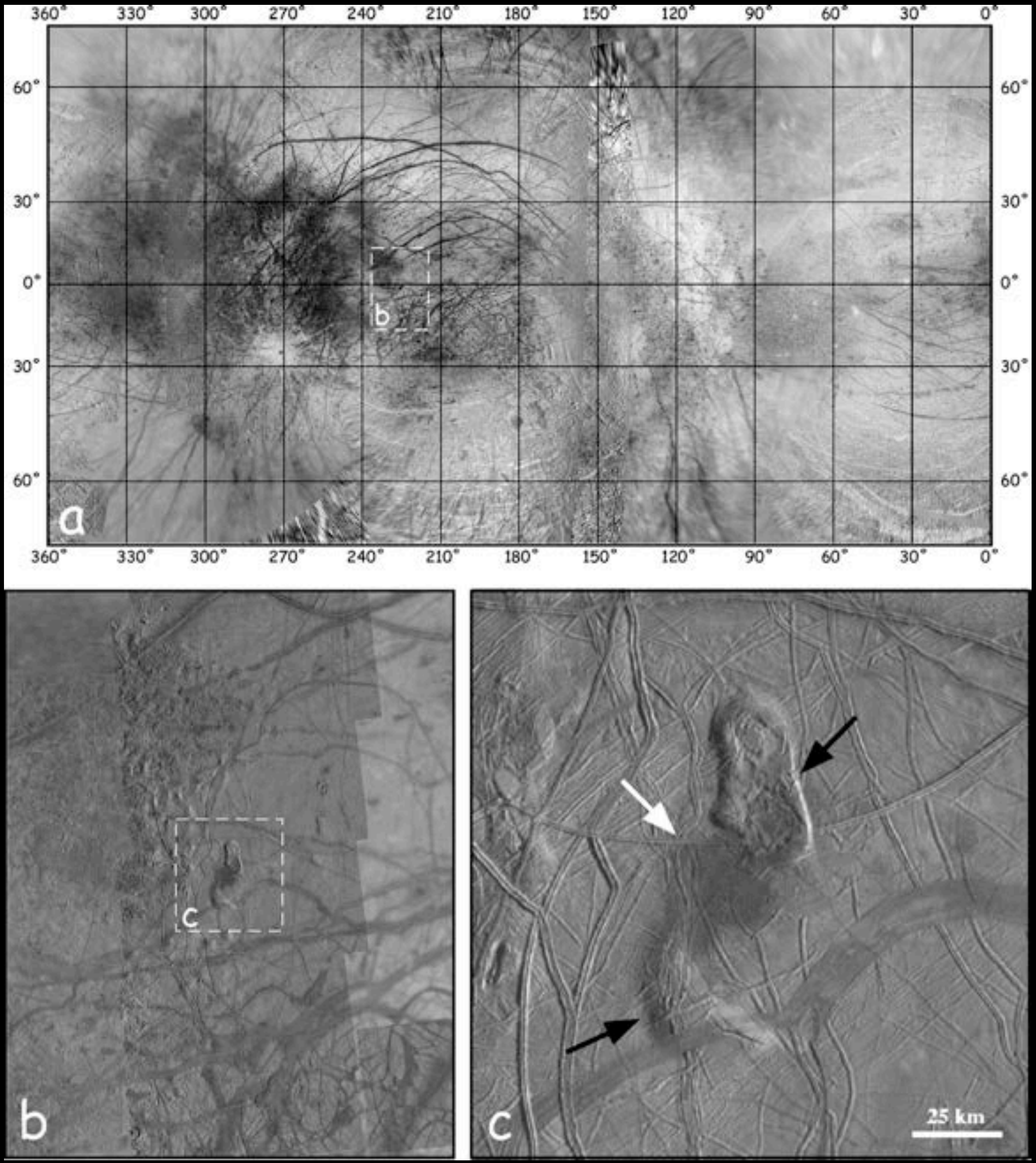

Prockter and Schenk, 2005

Castalia Macula

Northern dome = 900 m above surrounding ridged plains

Southern dome = 750 m

Castalia Macula = - 350 m

Total topographic amplitude = 1250 m

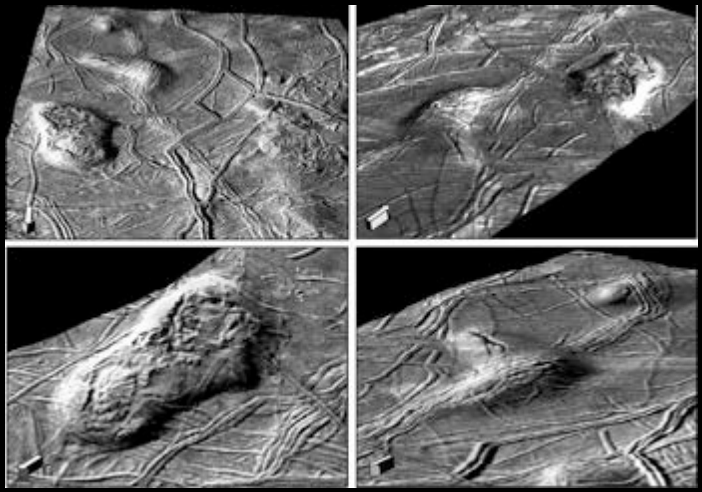

Figueredo et al.,2002

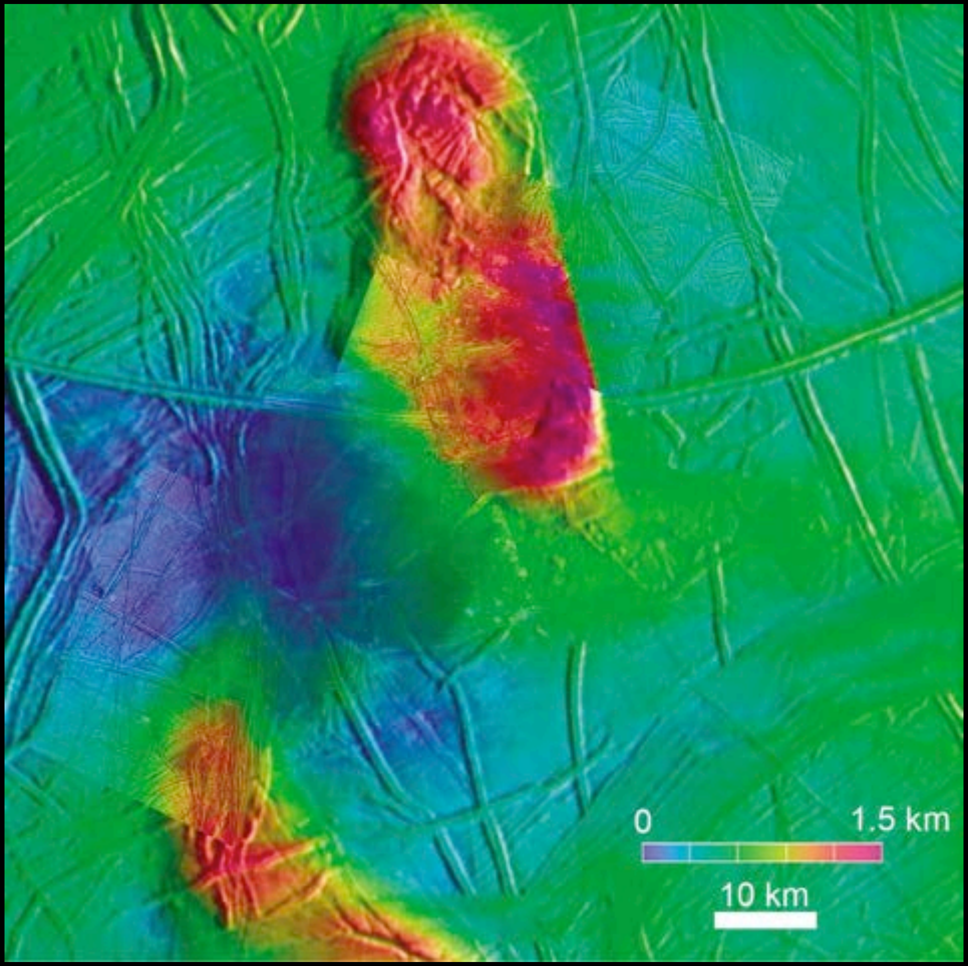

Prockter and Schenk, 2005

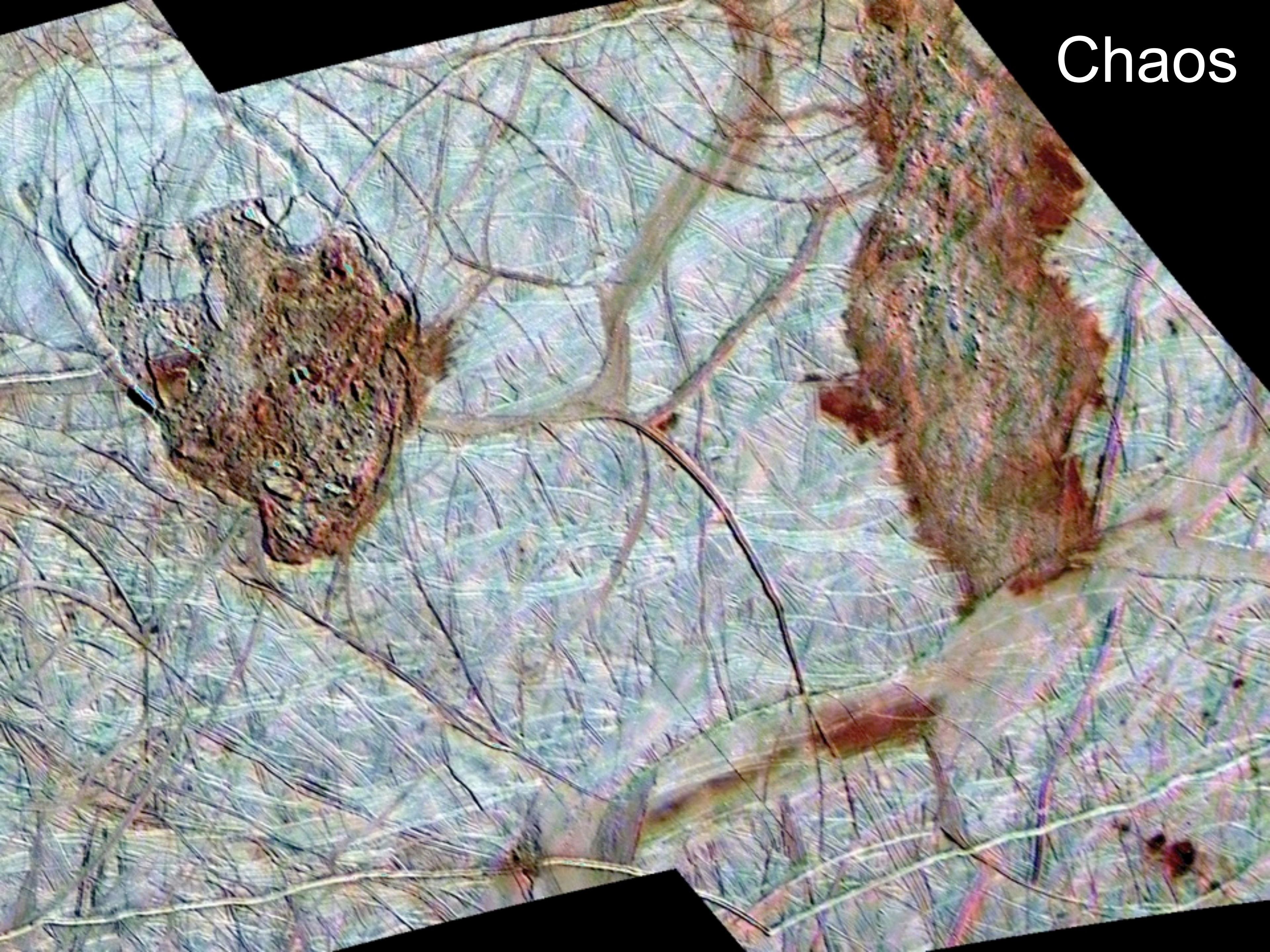
Chaos

Lenticulae

AKA pits, spots and domes

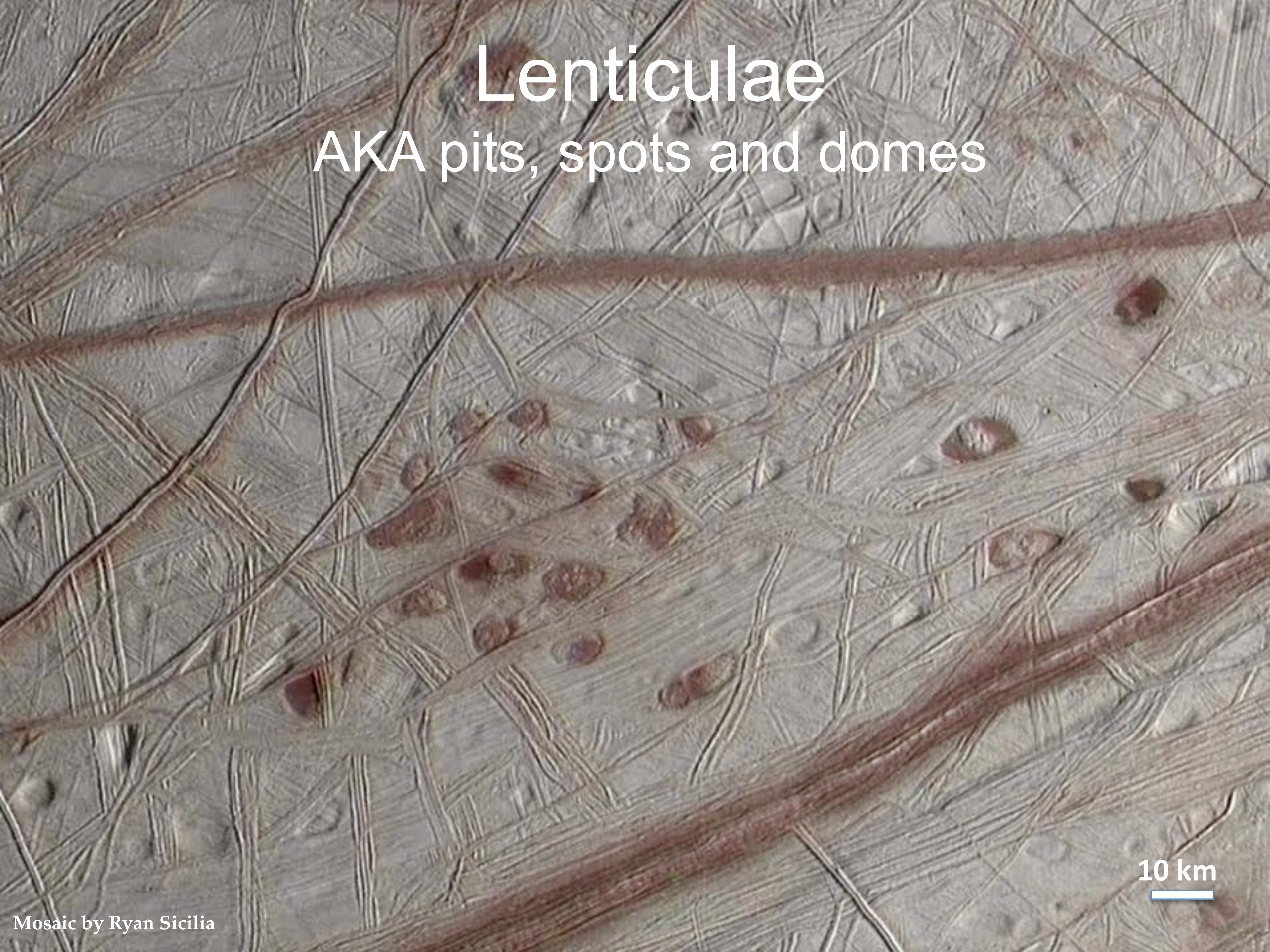

Lenticulae

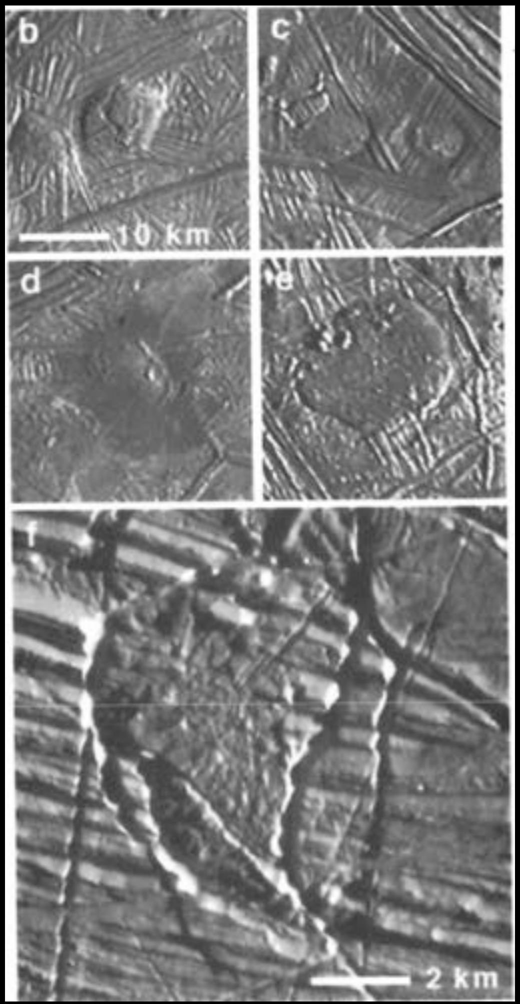

Pappalardo et al., 1999

Chaos

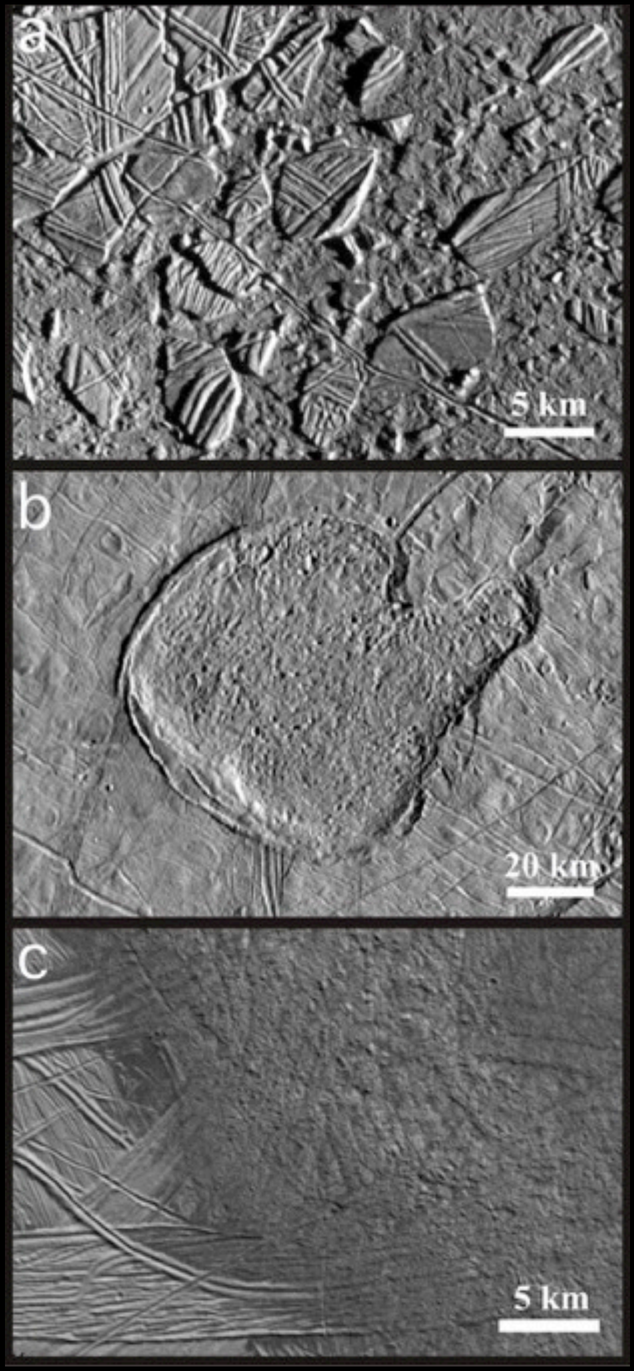

Convection in Europa's Ice Shell

- Chaos and lenticulae suggest convection of ice shell
- Ice shell can convect for small grain sizes (~1 mm), if tidally strained
- Warm (~240 K) plumes rise from base of ice in ~10^5 yr
- Compositional buoyancy needed to breach near-surface "stagnant lid"

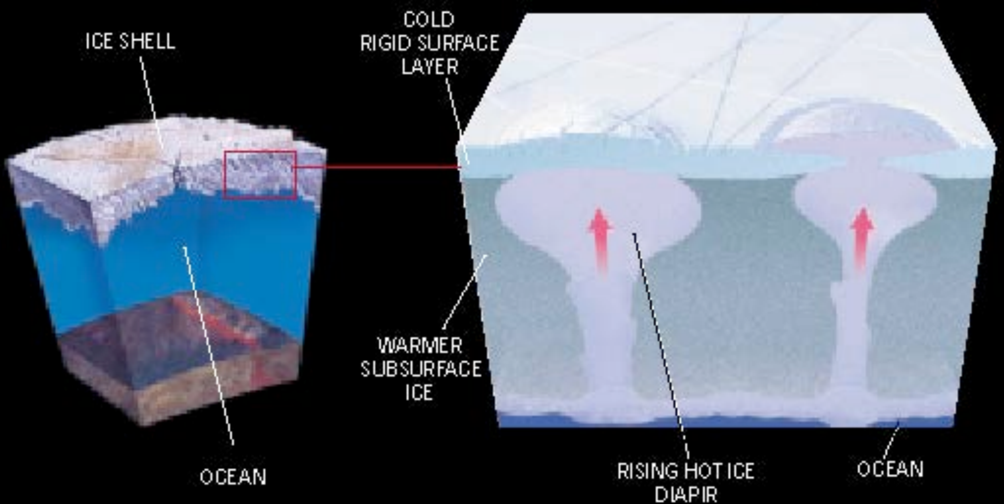

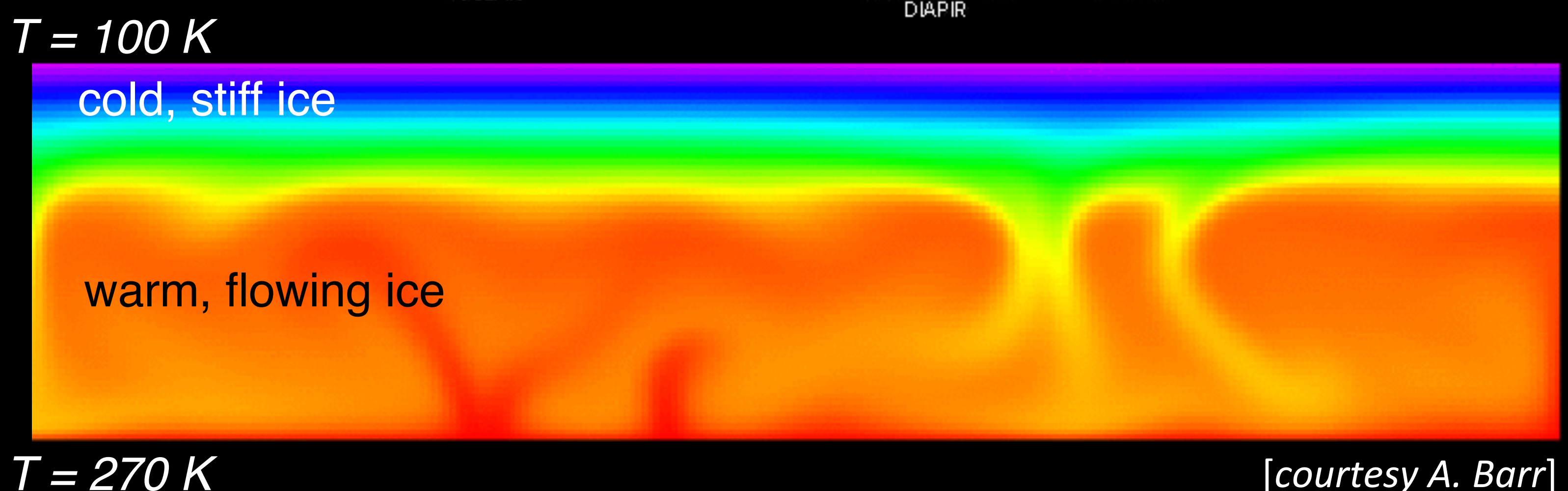

[*courtesy A. Barr*]

Conamara Chaos

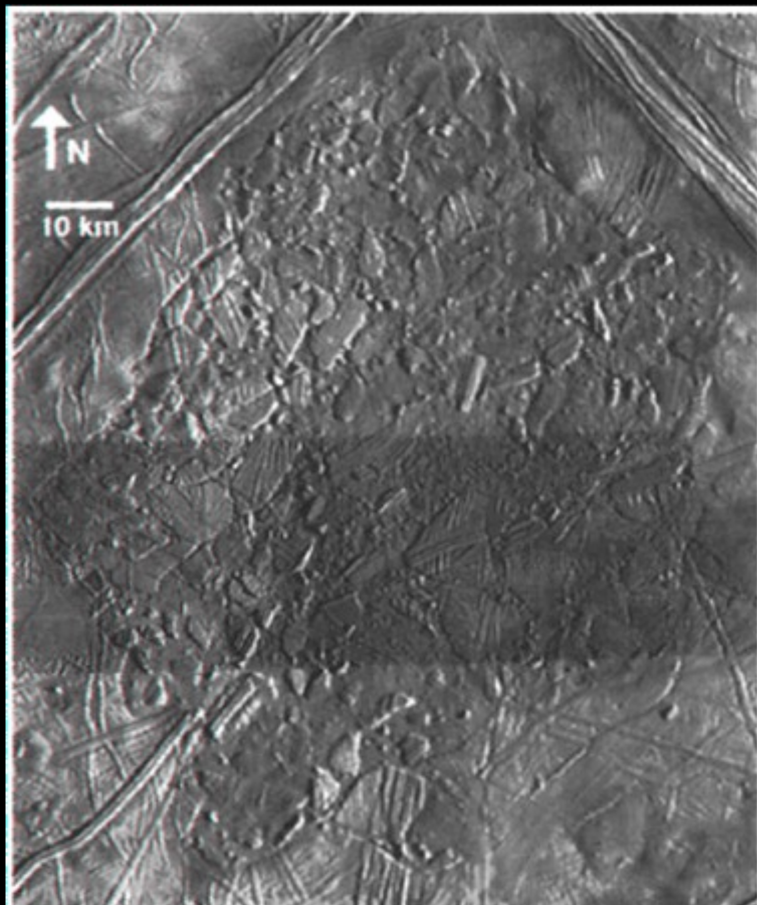

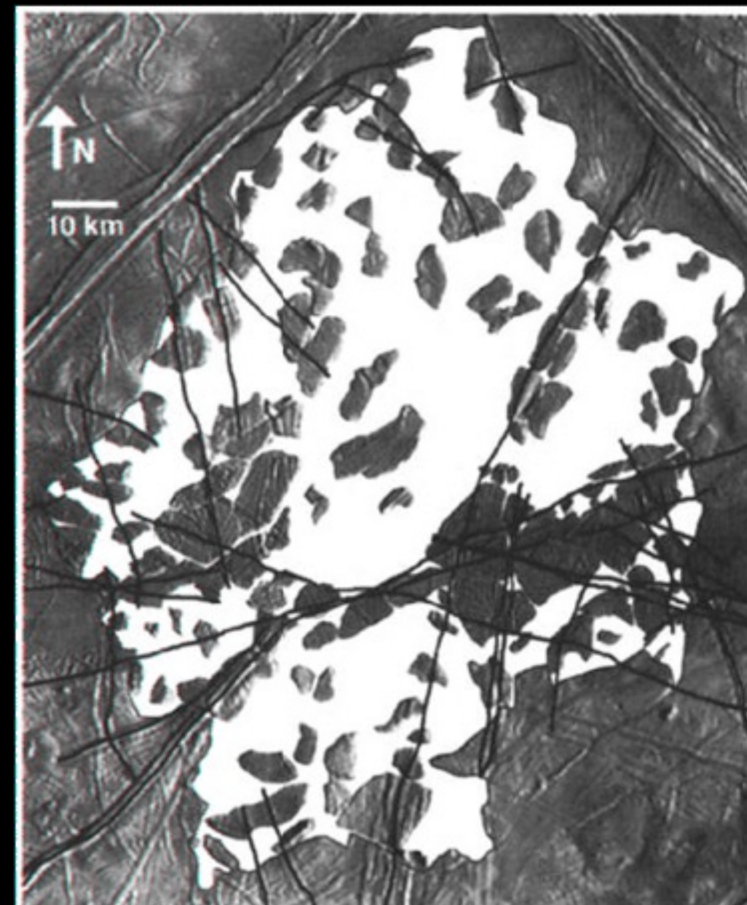

Spaun et al., 1998

~78% of the plates in Conamara have undergone horizontal translations, and 81% have rotated by on average 11º, implying elevated near-surface temperatures and a highly mobile substrate over lateral scales of ~ 100 km

Chaos endmember models

Melting model

Diapirism model

Candidate chaotic terrain formation models

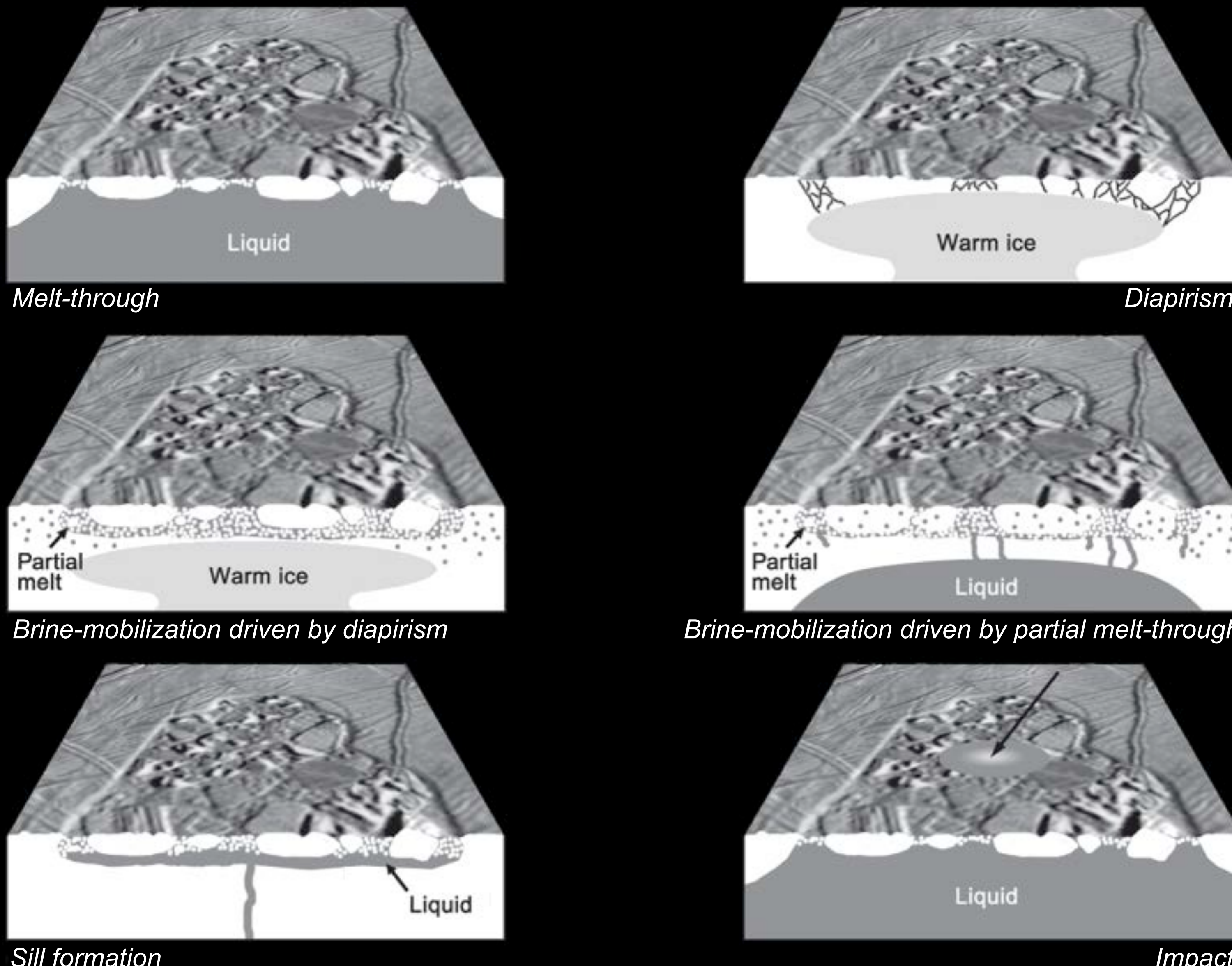

Colllins and Nimmo, 2007

Candidate chaotic terrain formation models

Melt-through

Diapirism

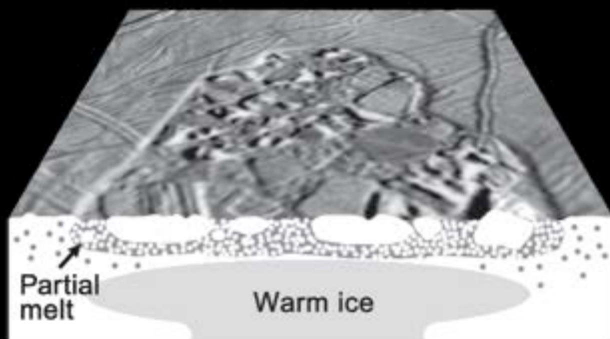

Brine-mobilization driven by diapirism

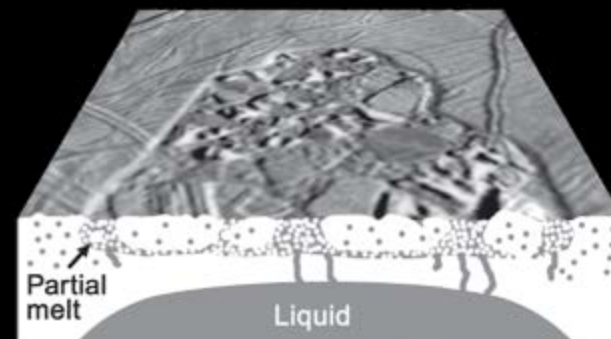

Brine-mobilization driven by partial melt-through

Sill formation

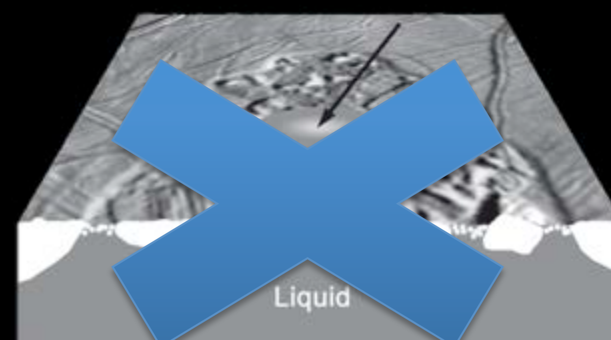

Impact

Colllins and Nimmo, 2007

Subsurface lakes in the ice shell

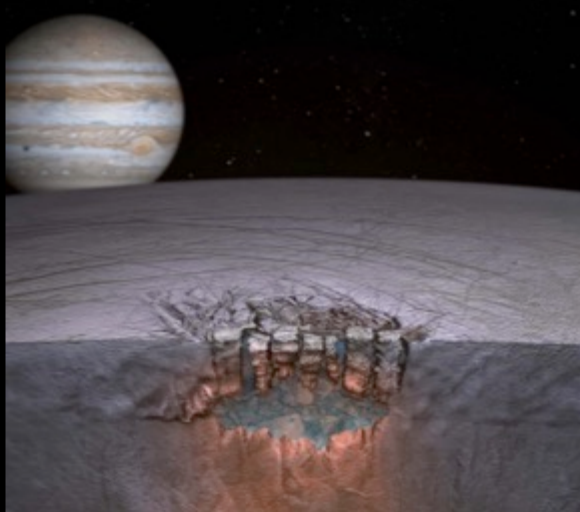

Using terrestrial analogs, Schmidt et al. (2011) showed that chaos matrix domes and depressions can be explained if they form above shallow subsurface (~3 km) lakes

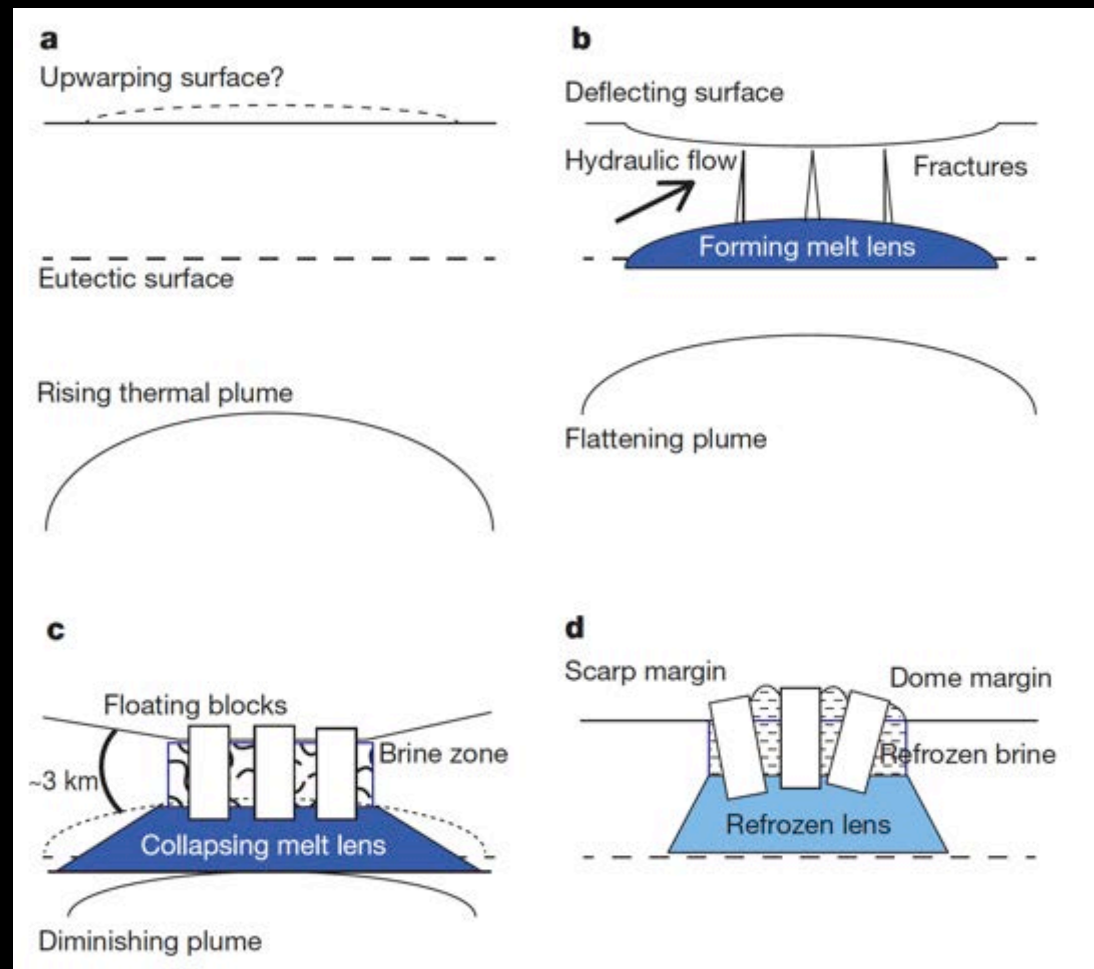

Schmidt et al., 2011

Pit and uplift modeling

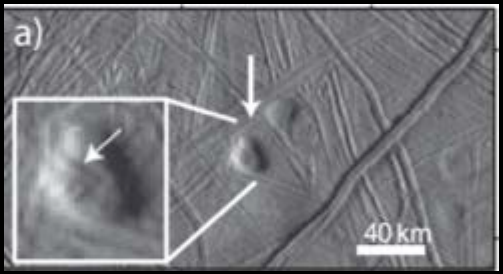

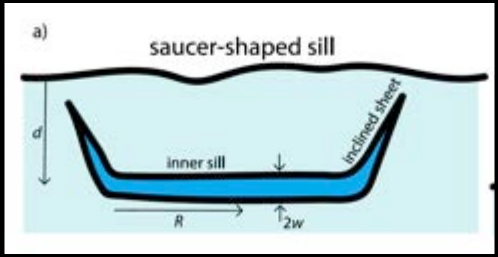

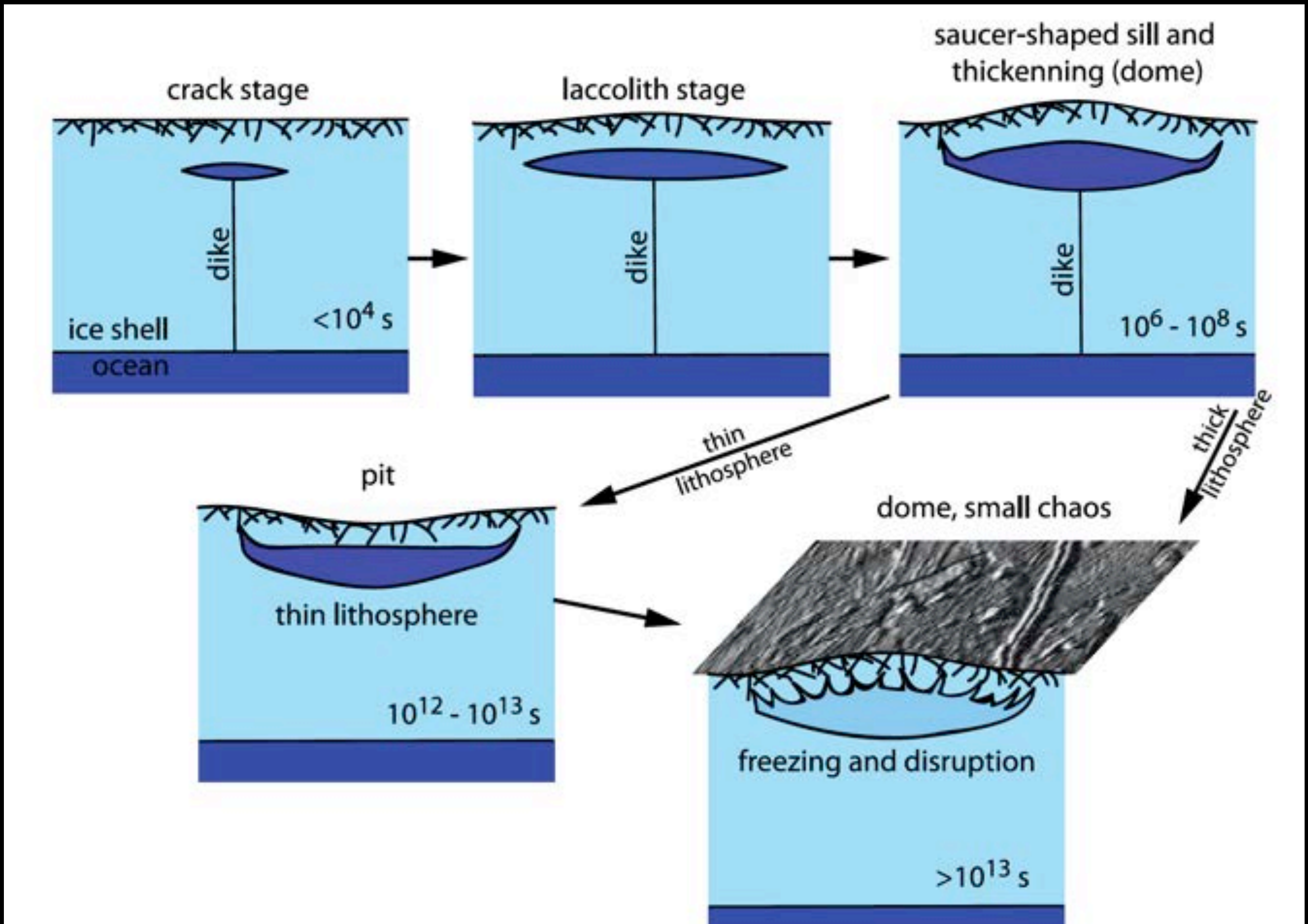

Manga and Michaut, 2016

- Modeling of saucer-shaped sills by Manga and Michaut (2016) explains the features of pits, spots, and domes, and suggests that intrusions are, or were 1-5 km below the surface
- Liquid water is predicted to exist presently under pits

Ice thickness estimates using impact features

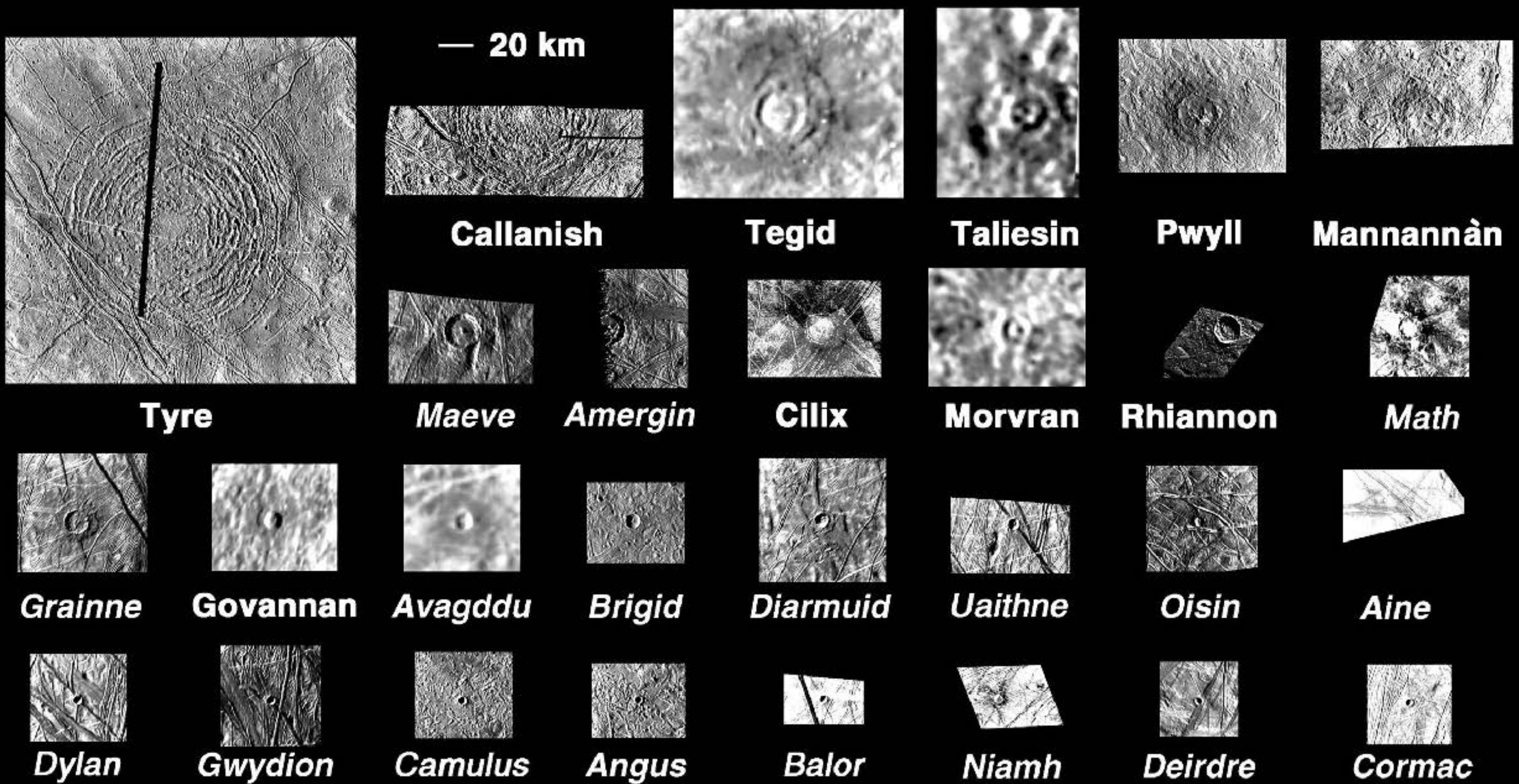

Moore et al., 2001

All impact features on Europa > 4 km in diameter

Impact Structures

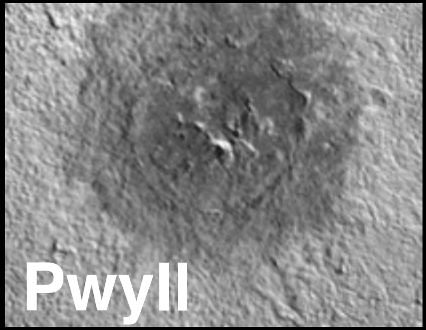

- Few large impact craters imply 40–90 Myr old surface
- Central peak craters show “relaxed” topography
- Multi-ringed impacts penetrated thick ice

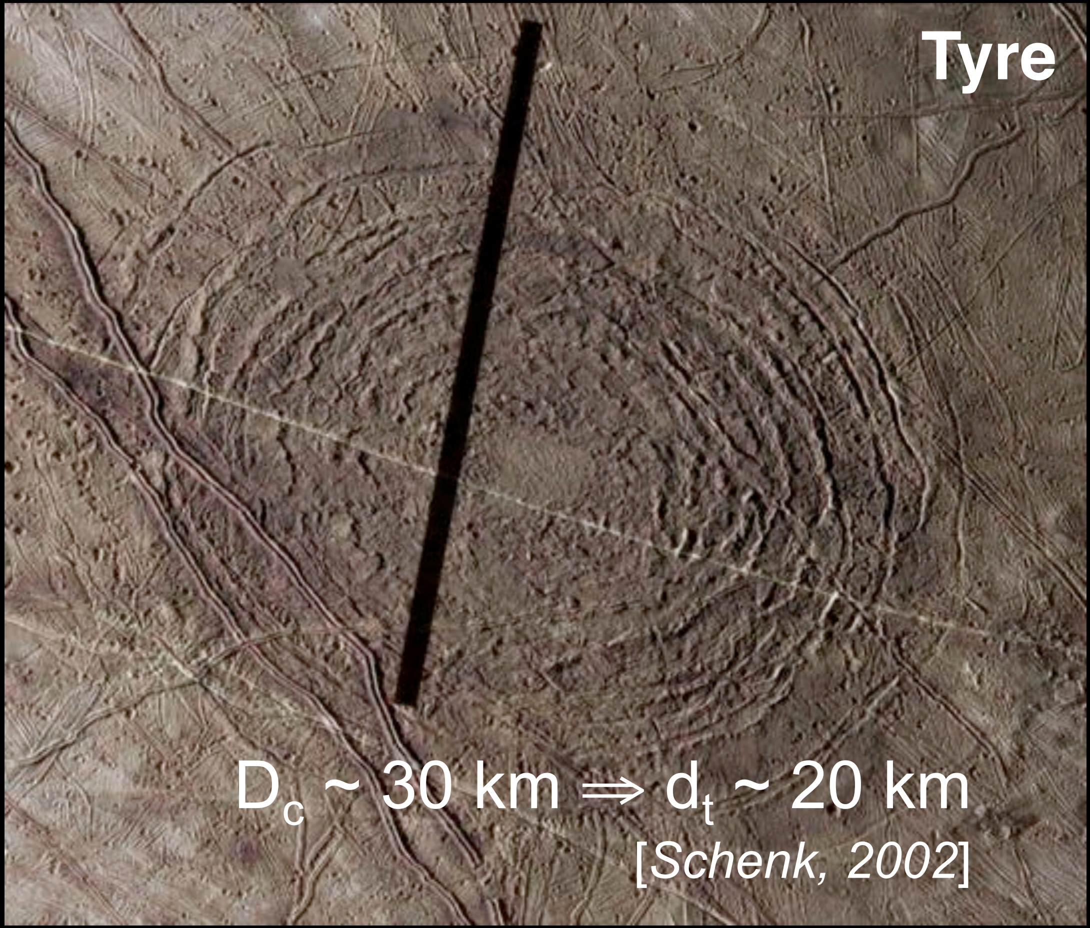

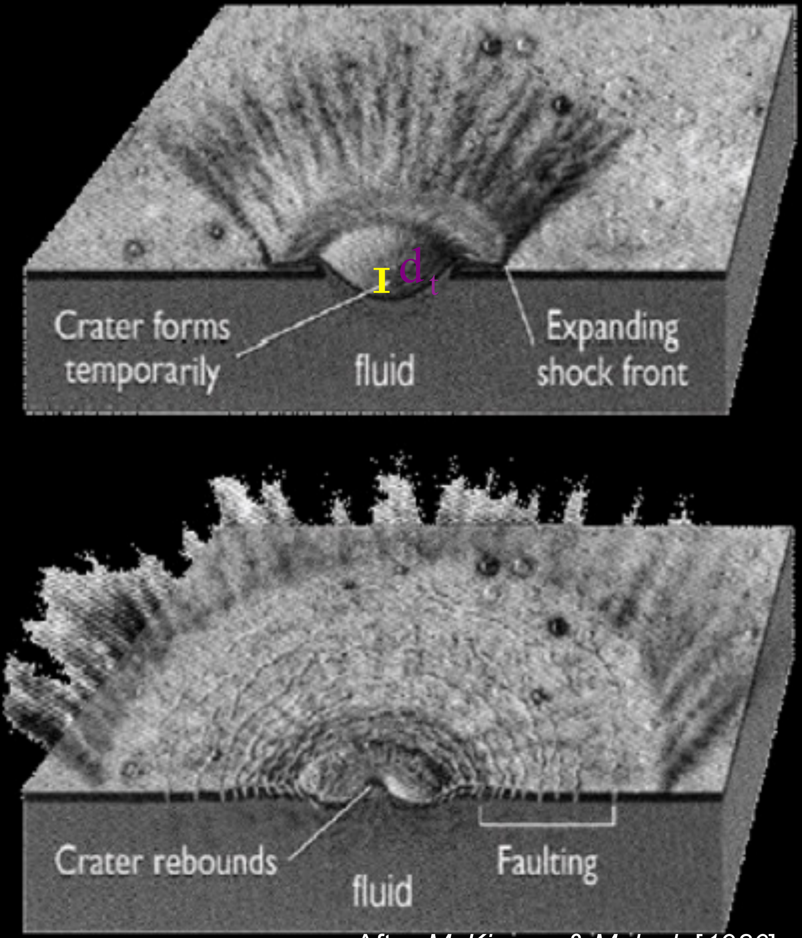

After *McKinnon & Melosh* [*1980*]

Large impacts

- Different basin morphologies are predicted depending on the thickness of the upper layer
- Ice thicknesses of >12-16 km are consistent with the formation of ring faults around craters like Tyre and Callanish (Turtle (1998)

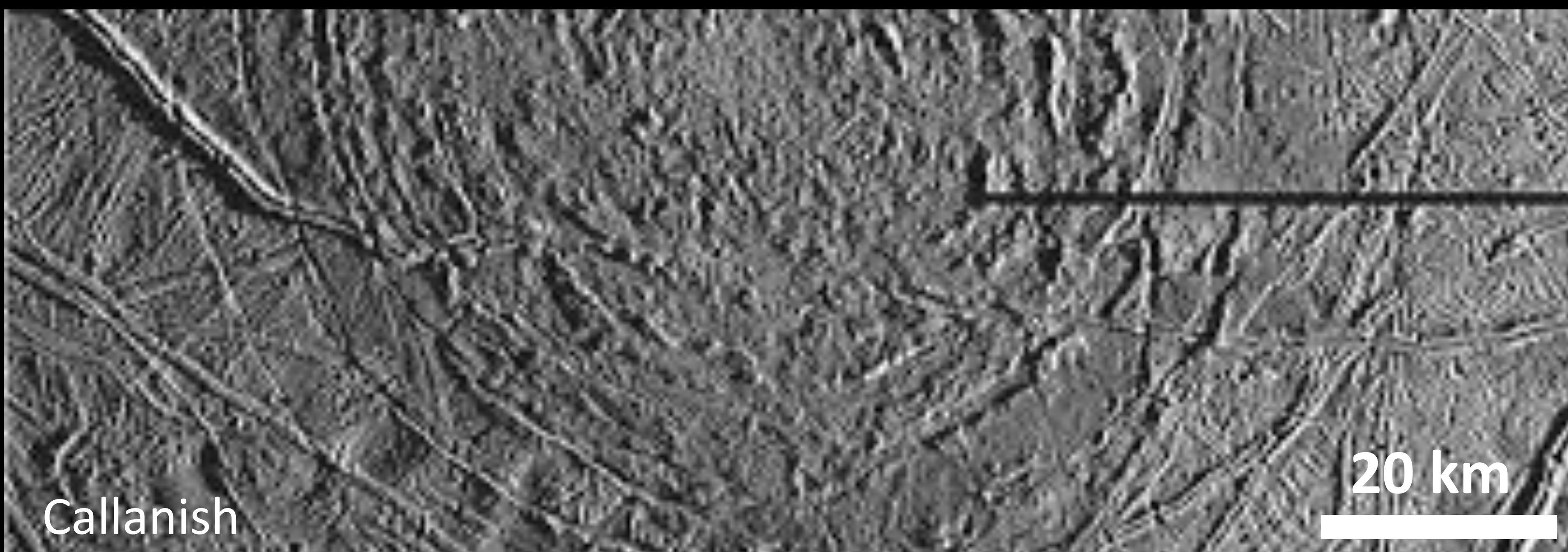

Central peak craters

- The transient crater diameter of Pwyll, one of Europa's youngest craters, is estimated to be ~ 16 km, implying that Europa's ice shell was at least 15 km thick when Pwyll formed
- Pwyll is nevertheless quite shallow, with a subdued floor. This small depth-to-diameter ratio may be due to the isostatic adjustment of large-scale topography facilitated by warm, plastically deformable ice at depth

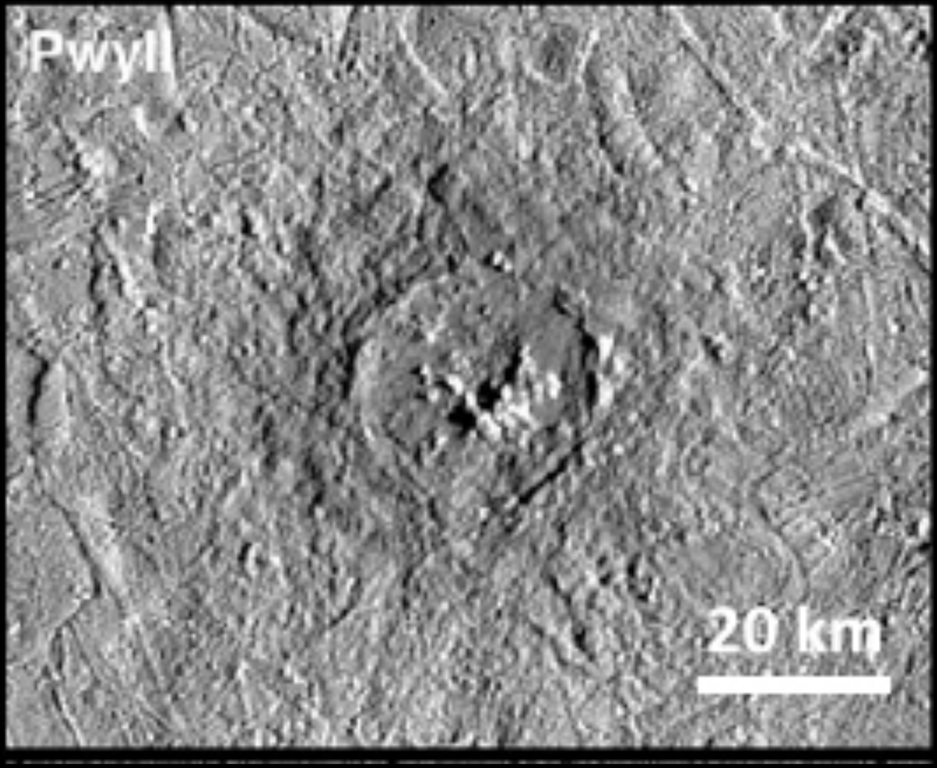

What can Europa's putative plumes tell us about the thickness of the shell?

- Hubble has observed hydrogen and oxygen ultraviolet glow, 200 km above Europa
- Indicates water plumes
- May be transient, perhaps linked to Europa's tidal cycle
- Source may be the ocean (although unlikely if shell is thick), a lake within the ice, or perhaps warm shallow ice

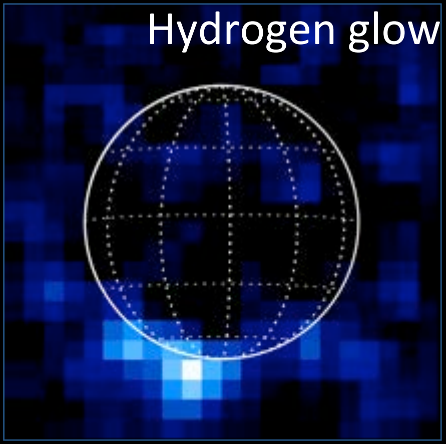

NASA/L. Roth

Ice shell thickness estimates: Mechanical - flexure

Estimates of ice shell thickness on Europa using a variety of mechanical, thermodynamic, cratering, and other methods

Citation	Model method	Location	Ice shell estimated thickness	Portion of shell modeled	Method assumptions and notes	Application to Androgeos Linea*
Mechanical methods: flexure						
Billings and Kattenhorn (this paper)	Flexure, line load	14.7° N, 273.4° W Androgeos Linea	520–2410 m	Elastic	Measured distance to maximum stress location (flanking cracks). Broken plate model. $E = 6 \times 10^7$–6×10^9 Pa, $\nu = 0.3$, $\rho_0 = 1186\ \mathrm{kg/m^3}$, $g = 1.35\ \mathrm{m/s^2}$.	520 m (for highest E value)
Billings and Kattenhorn (this paper)	Flexure, line load	8.4° N, 271° W Ridge R	216–1000 m	Elastic	As above.	520 m
Billings and Kattenhorn (this paper)	Flexure, line load	4.7° N, 325.7° W Ridge C2r	465–2160 m	Elastic	As above.	520 m
Chuang et al. (2001)	Flexure, line load	22° N, 82° W SW quadrant of Murias Chaos	~2.1–2.6 km	Elastic	Determined distance to forebulge by fitting model to topography. $E = 9.33$ GPa, $\nu = 0.325$, $\rho_0 = 1208\ \mathrm{kg/m^3}$.	449 m
Figueredo et al. (2002)	Flexure, cylindrical load on sphere	22° N, 82° W SW quadrant of Murias Chaos	~4 ± 2 km	Elastic	Fit model to topography. $E = 9$ GPa, $\nu = 0.325$, $\rho_0 = 1208\ \mathrm{kg/m^3}$.	454 m
Hurford et al. (2004)	Flexure, line load	Various ridges	~100–400 m	Elastic	Measured distances to forebulge using photoclinometry. Broken plate model. $E = 1$ GPa, $\rho_0 = 1055\ \mathrm{kg/m^3}$, $g = 1.35\ \mathrm{m/s^2}$.	908 m
Nimmo et al. (2003)	Flexure, distributed load	3° N, 182° W Cilix	6 km	Elastic	Measured forebulge distance using stereoscopic data. Fit model to topography. Continuous plate model. $E = 1$ GPa, $\rho_0 = 900\ \mathrm{kg/m^3}$.	861 m; 342 m cont.
Tufts (1998)	Flexure, line load	8.4° N, 271.3° W Ridge R	123–353 m	Elastic	Measured distance to forebulge based on the distortion of cross-cutting surface features. Broken plate model. $E = 1$–24 GPa, $\nu = 0.33$, $\rho_0 = 920\ \mathrm{kg/m^3}$, $g = 1.3\ \mathrm{m/s^2}$.	295 m
Williams and Greeley (1998)	Flexure, line load	W of Conamara in smooth band	150–500 m	Elastic	Measured forebulge distance from photoclinometry. Continuous plate model. $\rho_{\mathrm{liq}} = 1186\ \mathrm{kg/m^3}$, E on higher end of range of 6×10^7–6×10^9 Pa, $\nu = 0.3$, $g = 1.35\ \mathrm{m/s^2}$.	520 m; 206 m cont.
Williams and Greeley (1998)	Flexure, distributed load	W of Conamara in smooth band	100–350 m	Elastic	$\rho_{\mathrm{liq}} = 1186\ \mathrm{kg/m^3}$, $\rho_{\mathrm{ice}} = 1126$, $\rho_{\mathrm{load}} = 1510$. E on higher end of range of 6×10^7–6×10^9 Pa; $\nu = 0.3$, $g = 1.35\ \mathrm{m/s^2}$.	520 m; 206 m cont.

* Re-calculated ice thickness at Androgeos Linea using values for E, ν, ρ_0, and g, if provided, by the cited researcher. If a range in E was cited, only the high end of the range was used; when no value was given for a parameter, values were used from Billings and Kattenhorn. A broken plate model was used for comparison calculations; in addition, a continuous plate model result was calculated where also used by the original researcher.

Billings and Kattenhorn, 2005

Ice shell thickness estimates: Mechanical - non-flexure

Citation	Model method	Location	Ice shell estimated thickness	Portion of shell modeled	Method assumptions and notes
			Mechanical methods: other than flexure		
Carr et al. (1998)	Buoyancy	13° N, 273° W Conamara	⩾2 km	Total	Results are the minimum thickness if rafts are floating in liquid water. No input values given.
Carr et al. (1998)	Dimension of chaos rafts	13° N, 273° W Conamara	⩽"Few km"	Brittle	Thickness is probably ⩽ horizontal dimensions of smallest plates that retain original surface features.
Golombek and Banerdt (1990)	Structural integrity of undeformed, mobile ice rafts	Anti-jovian, Wedges region	3–6 km	Brittle	Lower limit from observation of rotation of blocks; upper limit is from available driving stress to overcome lithostat.
Greeley et al. (1998)	Structural integrity of undeformed, mobile ice rafts	Unspecified	<"Few km"	Total	Used "plate dimensions".
Greenberg et al. (2000)	Lithostatic stress constraints	Global	<"Few km"	Total = brittle	Cracks penetrate to liquid and are caused by tidal stresses.
Hoppa et al. (1999a)	Lithostatic stress constraints	Global	<"Few km"	Total = brittle	Cycloidal cracks penetrate to liquid and are caused by tidal stresses. Water ice shear mod. $\mu = 3.52$ GPa; $\nu = 0.33$; diurnal stress $\sigma_{\max} = 40$ kPa.
Kadel et al. (2000)	Buoyancy (isostacy of rafts in liquid)	34° N, 144° W chaos at Tyre	0.9–5.5 km	Total	Raft height $h = 240$–290 m. Briny ice in briny liquid, $\rho_{\text{ice}} = 927$ (pure water ice) to $1126\ \text{kg/m}^3$ (briny ice); $\rho_{\text{liq}} = 1186\ \text{kg/m}^3$ (briny liquid).
Kadel and Greeley (2000)	Buoyancy (isostacy of rafts in liquid)	16.44° N–10° N 11 rafts	2.10 km	Total	Raft height $h_{\text{ave}} = 106$ m for chaos features in latitude range. Other parameters as above.
Kadel and Greeley (2000)	Buoyancy (isostacy of rafts in liquid)	0° N–10° N 60 rafts	1.27 km	Total	Raft height $h_{\text{ave}} = 120$ m for chaos features in latitude range. Other parameters as above.
Kadel and Greeley (2000)	Buoyancy (isostacy of rafts in liquid)	10° N–20° N 6 rafts	3.64 km	Total	Raft height $h_{\text{ave}} = 184$ m for chaos features in latitude range. Other parameters as above.
Kadel and Greeley (2000)	Buoyancy (isostacy of rafts in liquid)	20° N–30° N 13 rafts	5.85 km	Total	Raft height $h_{\text{ave}} = 296$ m for chaos features in latitude range. Other parameters as above.
Kadel and Greeley (2000)	Buoyancy (isostacy of raft in liquid)	30° N–40° N 18 rafts	4.29 km	Total	Raft height $h_{\text{ave}} = 217$ m for chaos features in latitude range. Other parameters as above.
Kadel and Greeley (2000)	Buoyancy (isostacy of raft in liquid)	40° N–50° N 4 rafts	5.91 km	Total	Raft height $h_{\text{ave}} = 299$ m for chaos features in latitude range. Other parameters as above.
Lucchitta and Soderblom (1982)	Structural integrity of undeformed, mobile ice rafts	Global	⩾"A few km" ⩽"A few tens of km"	Total	Lower limit based on structural integrity (lack of deformation) of rotated blocks. Upper limit based on evidence ocean–surface interaction.
Schenk and McKinnon (1989)	Structural integrity of undeformed, mobile ice rafts/lithostatic stress constraints	Anti-jovian, Wedges region	"A few"–10 km	Brittle	Lower limit is based on Lucchitta and Soderblom (1982). Upper limit is based on the maximum depth a tidal stress-induced crack can penetrate.
Williams and Greeley (1998)	Buoyancy (isostacy of blocks in liquid)	13° N, 273° W Conamara	0.8–2.9 km	Total	Block height $h = 40$–150 km. Briny ice in briny liquid, $\rho_{\text{ice}} = 1126\ \text{kg/m}^3$, $\rho_{\text{liq}} = 1186\ \text{kg/m}^3$.

Billings and Kattenhorn, 2005

Ice shell thickness estimates: Impact cratering

Citation	Model method	Location	Ice shell estimated thickness	Portion of shell modeled	Method assumptions and notes
			Impact cratering analyses		
Greeley et al. (1998)	Transient crater depth, crater morphology	25° S, 271° W Pwyll	⩾10–15 km	Total	Based on the calculated transient crater depth and the observation of crater morphology (including central peaks), implying that the impactor did not penetrate the ice shell.
Kadel et al. (2000)	Scaling of transient crater depth based on diameter	34° N, 144° W Tyre	3.5 ± 0.5 km	Total	Impactor penetrated to fluid layer.
Moore et al. (1998)	Impact modeling and crater morphology	Callanish, Tyre	~6–15 km	Total	Ice layer overlies low-viscosity layer. Impactor penetrated the ice layer and radial stresses in top layer caused fracturing in concentric rings around impact site.
Moore et al. (1998)	Impact modeling and crater morphology	Pwyll	~10–15 km	Total	Ice layer overlies low-viscosity layer. Impactor did not penetrate the ice layer.
Moore et al. (2001)	Transient crater depth/morphology	2° S, 180° W Cilix	⩾2.4–4.7 km	Total	Based on the calculated transient crater depth and the observation of a central peak complex, implying that the impactor did not penetrate the ice shell.
Moore et al. (2001)	Transient crater depthmorphology	3° N, 240° W Manannán	⩾2.86–5.47 km	Total	Based on the calculated transient crater depth and the observation of interior massifs, implying that the impactor did not penetrate the ice shell.
Moore et al. (2001)	Transient crater depth/morphology	34° N, 146° W Tyre	⩾5.59–9.98 km	Total	Based on the calculated transient crater depth and the observation of crater morphology (including no central peaks), implying that the impactor did penetrate the ice shell.
Moore et al. (2001)	Transient crater depth/morphology	25° S, 271° W Pwyll	⩾2.6–3.6 km	Total	Based on the calculated transient crater depth and the observation of crater morphology (including central peaks), implying that the impactor did not penetrate the ice shell.
Schenk (2002)	Crater morphology	Global	19 km	Total	Results are a lower boundary. Morphology variations are due to depth of penetration through the total ice layer. Calculated transient crater depth based on crater diameter.
Turtle and Pierazzo (2001)	Impact modeling and crater morphology	Numerous impact sites	>3–4 km	Total	Model is for ice layer over water. Results are a lower boundary. The transient crater diameter is estimated from the observed final crater diameter.
Turtle and Ivanov (2002)	Impact modeling and crater morphology	Various small complex craters	⩾5–7 km	Total	As above.
Turtle and Ivanov (2002)	Impact modeling and crater morphology	Various large complex craters	⩾12–18.5 km	Total	As above.

Billings and Kattenhorn, 2005

Ice shell thickness estimates: Thermodynamic analyses

Citation	Model method	Location	Ice shell estimated thickness	Portion of shell modeled	Method assumptions and notes
			Thermodynamic analyses		
Hussmann et al. (2002)	Thermal equilibrium	Global	~32–38 km	Total	Calculates equilibrium thickness for tidal dissipation assuming a Maxwell rheology in a convecting ice layer that is overlain by a conducting stagnant lid and elastic layer. Implies a heat flow of ~20 mW/m^2 and a melting point viscosity of ~10^{13}–10^{14} Pa s.
McKinnon (1999)	Convection modeling: initiation of convection	15° N, 270° W Conamara Chaos	~6–26 km	Total	Constrains thickness for convection to occur. Applies temperature-dependent viscosity convection scaling. Shell assumed to be pure water ice. Shows convection is possible for ice shells <30 km thick. Presumes that shell thinning and thermal runaways could occur if convecting, tidally heated shell exists.
Nimmo et al. (2003)	Temperature gradient through ice shell	3° N, 182° W Cilix	15 km	Total	Based on elastic thickness of 6 km from flexural analysis, $E = 1$ GPa, $\rho_0 = 900$ kg/m^3. Convecting ice layer underlies brittle layer.
Ojakangas and Stevenson (1989)	Thermal equilibrium	Global (averages)	13–25 km	Total	Range includes calculations using both Maxwell and generalized heat flow rheologies.
Pappalardo et al. (1998)	Initiation of convection	Global	~3–10 km	Total	Applies a parameterized convection approach to constrain the thickness of a convecting layer, to which a ⩽2 km thick conductive lid is added. Results are thickness at which convection can initiate.
Quick and Marsh (2015)			28 km		
Rathbun et al. (1998)	Convection: diapir rise time	15° N, 270° W Conamara Chaos region	<"Few tens of km"	Total	Dome features are caused by diapirs and size is related to diapir size; size of domes limits depths from which diapirs can originate.
Sotin et al. (2004)	Thermal equilibrium	Global	17–29 km	Total	Range is geographic, from equator to poles. Uses a Maxwell rheology. Both tidal and radiogenic heating contribute.
			Other methods		
Nimmo (2004b)	Force balance during rifting	Global	<15 km	Total	Utilized a technique developed for terrestrial rift modeling. Assumed a constant strain rate and a conducting shell.
Pappalardo et al. (1999)	Terrestrial analog approach	8.4° N, 271.3° W	1–2 km	Brittle (seismic)	On earth, effective elastic lithospheric thickness = 20–40% of actual (seismic) thickness of brittle lithosphere due to weakening by faults; effective elastic thickness = ~400 m.
Tufts (1998)	Terrestrial analog approach	8.4° N, 271.3° W Ridge R	0.25–3.5 km	Total	Assumes elastic thickness = 10–50% of the total lithospheric thickness based on terrestrial analogy.

Billings and Kattenhorn, 2005

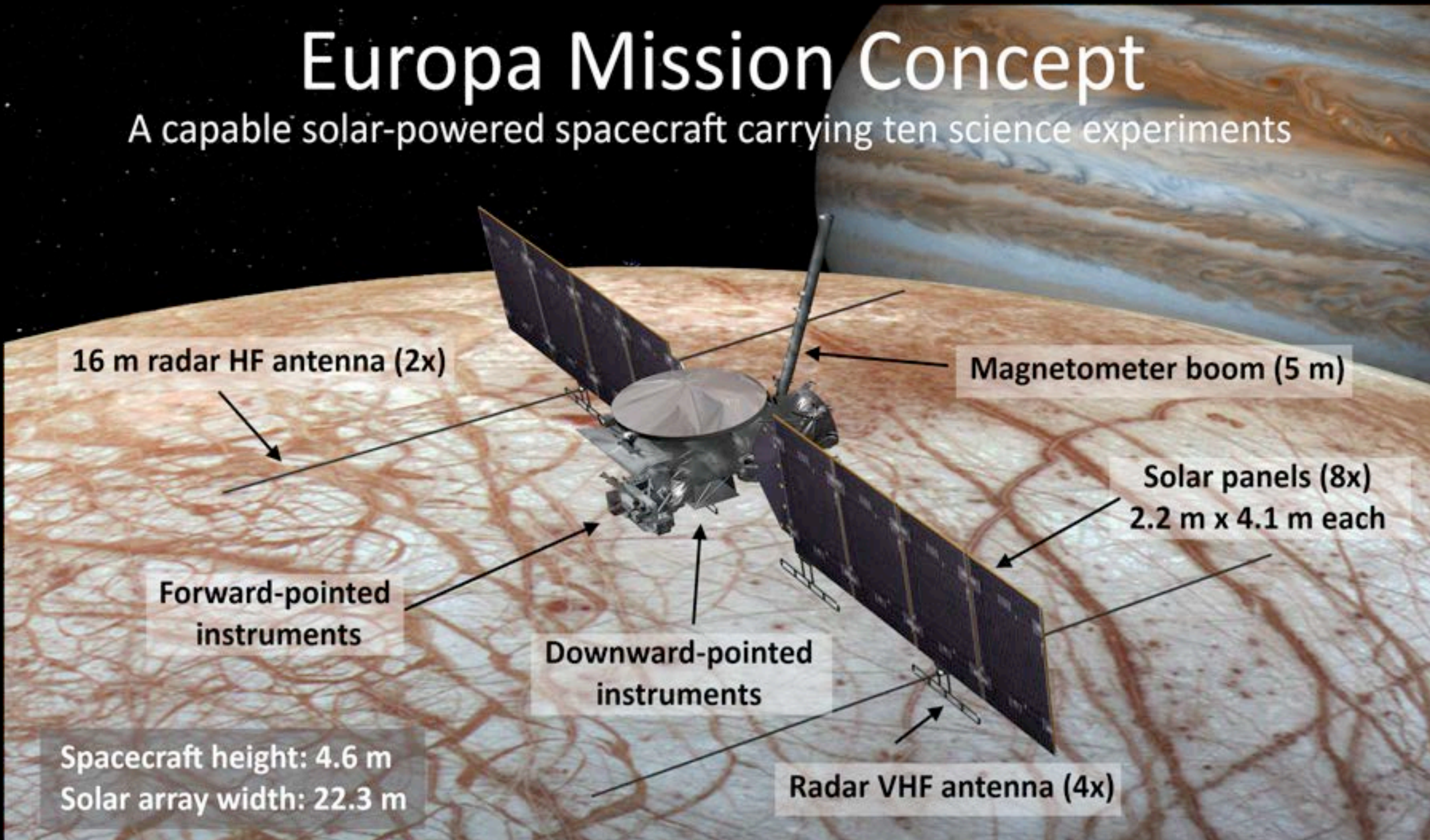
Europa Mission Concept
A capable solar-powered spacecraft carrying ten science experiments
16 m radar HF antenna (2x)
Magnetometer boom (5 m)
Solar panels (8x)
2.2 m x 4.1 m each
Forward-pointed
instruments
Downward-pointed
instruments
Spacecraft height: 4.6 m
Solar array width: 22.3 m
Radar VHF antenna (4x)

Mission concept

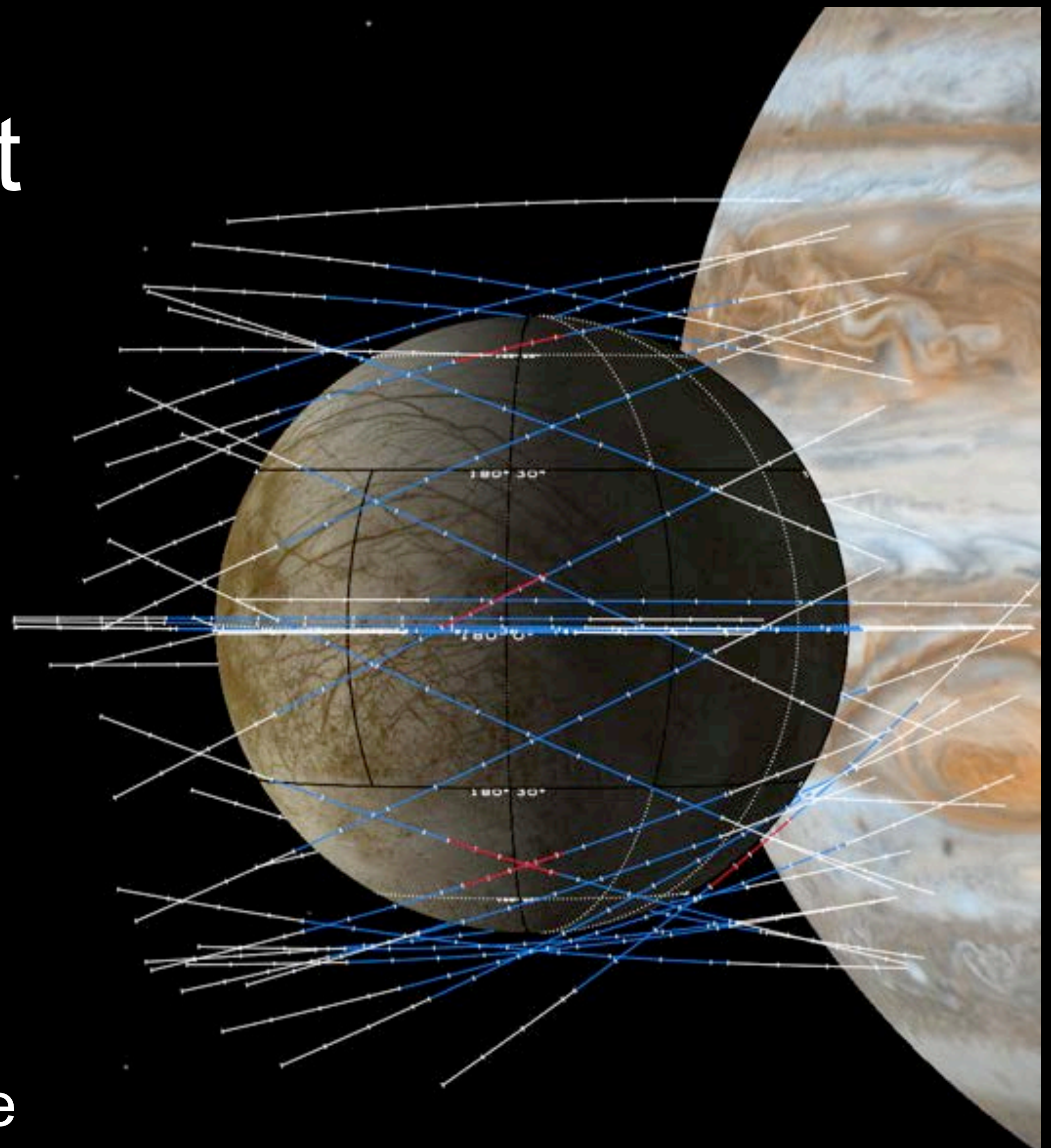

- Launch 2022, arrive as early as 2025
- 3-year primary mission, includes >42 encounters with Europa
- Multiple flybys of Europa build up global-regional coverage while minimizing radiation dose

Europa Multiple-Flyby Mission Science Goal and Objectives

Goal: **Explore Europa to investigate its habitability**

Objectives:

– **Ice Shell and Ocean:** Characterize the ice shell and any subsurface water, including their heterogeneity, ocean properties, and the nature of surface-ice-ocean exchange

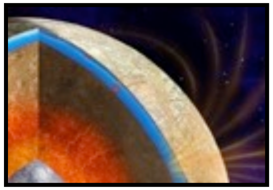

– **Composition:** Understand the habitability of Europa's ocean through composition and chemistry

– **Geology:** Understand the formation of surface features, including sites of recent or current activity, and characterize high science interest localities

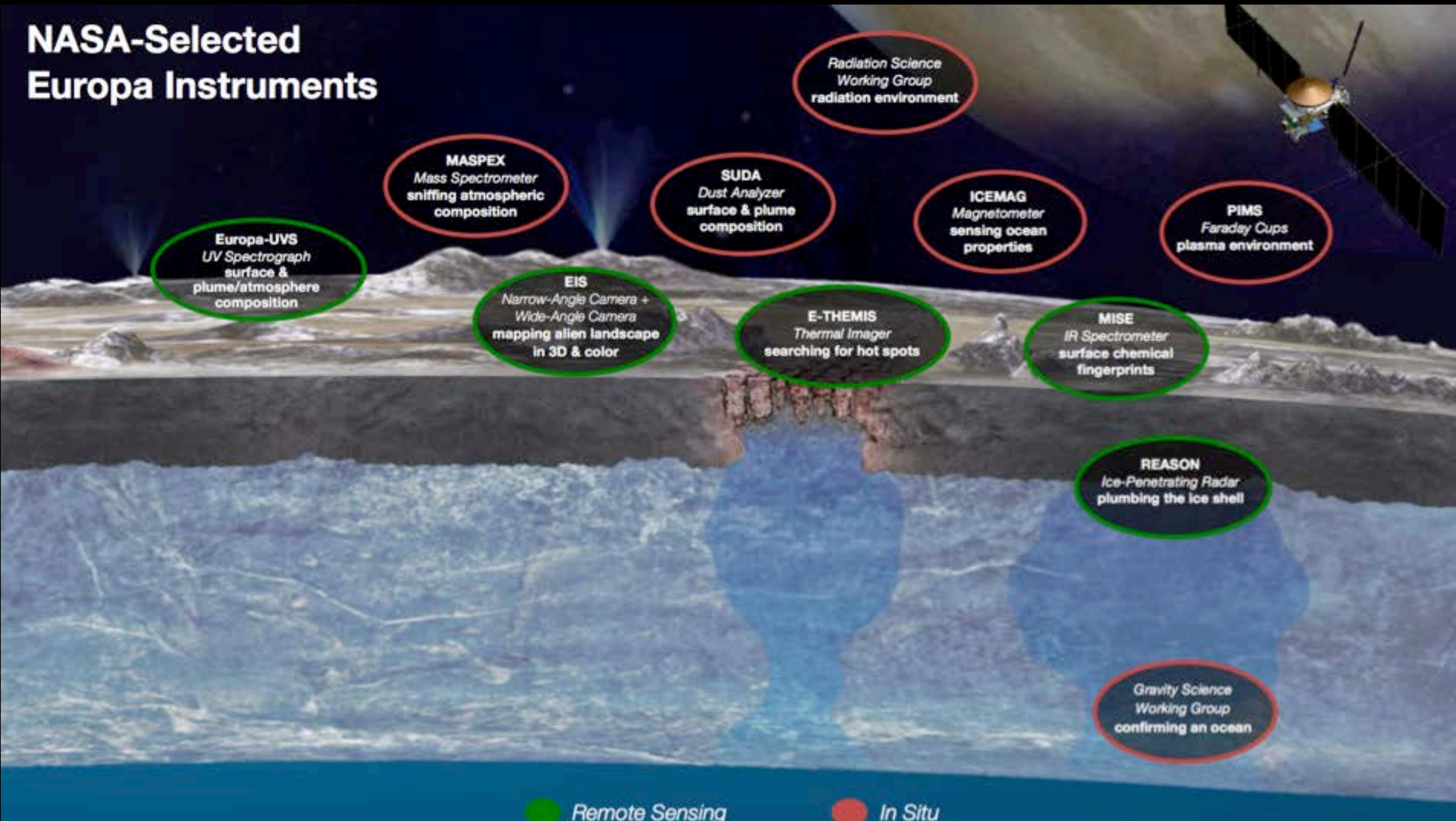

NASA-Selected
Europa Instruments
Radiation Science
Working Group
radiation environment
MASPEX
Mass Spectrometer
sniffing atmospheric
composition
SUDA
Dust Analyzer
surface & plume
composition
ICEMAG
Magnetometer
sensing ocean
properties
PIMS
Faraday Cups
plasma environment
Europa-UVS
UV Spectrograph
surface &
plume/atmosphere
composition
EIS
Narrow-Angle Camera +
Wide-Angle Camera
mapping alien landscape
in 3D & color
E-THEMIS
Thermal Imager
searching for hot spots
MISE
IR Spectrometer
surface chemical
fingerprints
REASON
Ice-Penetrating Radar
plumbing the ice shell
Gravity Science
Working Group
confirming an ocean
Remote Sensing
In Situ

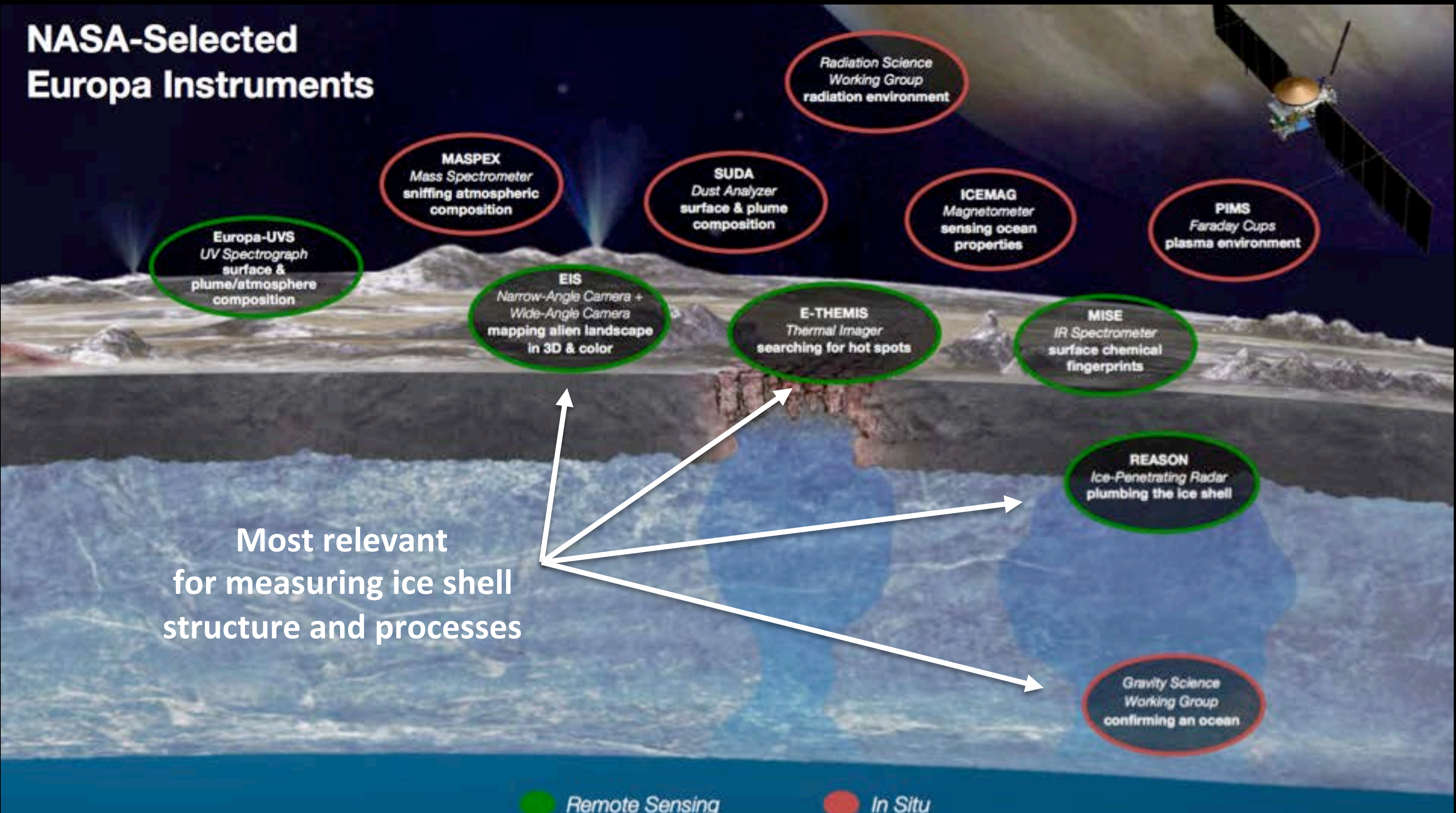
NASA-Selected
Europa Instruments
Radiation Science
Working Group
radiation environment
MASPEX
Mass Spectrometer
sniffing atmospheric
composition
SUDA
Dust Analyzer
surface & plume
composition
ICEMAG
Magnetometer
sensing ocean
properties
PIMS
Faraday Cups
plasma environment
Europa-UVS
UV Spectrograph
surface &
plume/atmosphere
composition
EIS
Narrow-Angle Camera +
Wide-Angle Camera
mapping alien landscape
in 3D & color
E-THEMIS
Thermal Imager
searching for hot spots
MISE
IR Spectrometer
surface chemical
fingerprints
REASON
Ice-Penetrating Radar
plumbing the ice shell
Most relevant
for measuring ice shell
structure and processes
Gravity Science
Working Group
confirming an ocean
Remote Sensing
In Situ

Europa Imaging System (EIS)

Zibi Turtle, Johns Hopkins U. Applied Physics Laboratory (APL)

- Constrain the formation of surface features and potential for current activity
- Characterize the ice shell
- Characterize the surface regolith at small scales

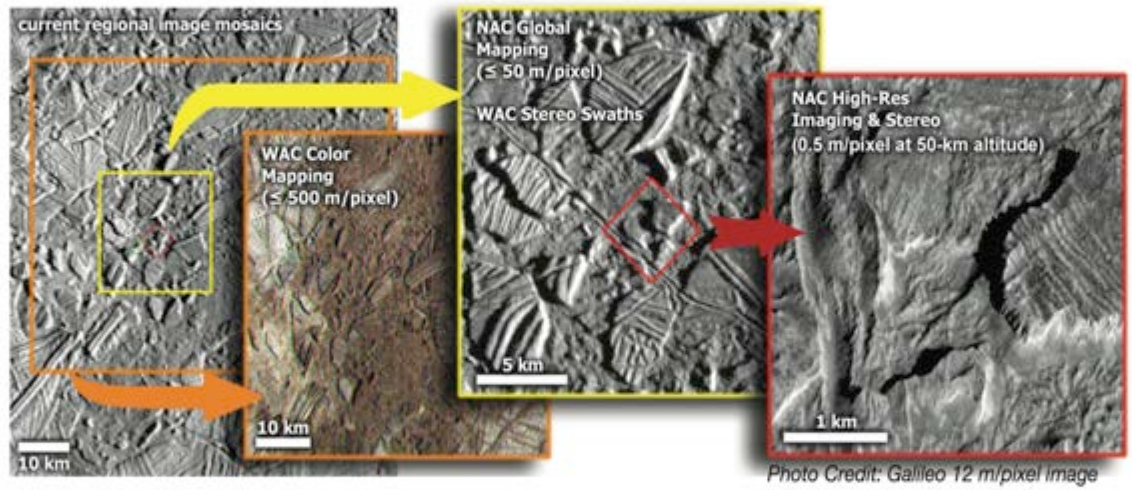

- NAC: high-resolution, stereo imaging, color
- NAC gimbal permits independent targeting, enabling near-global mapping, including stereo, and high-phase observations to search for potential plumes
- WAC: along-track stereo and color context imaging
- WAC supports cross-track clutter characterization for ice-penetrating radar

Key Instrument Parameters

	NAC	WAC
Detector	4096 × 2048 rad-hard CMOS	
Wavelength Range	Panchromatic plus 6 filters (350 – 1050 nm)	
Instantaneous Field of View	10 µrad (0.5 m/pixel at 50 km)	218 µrad (11 m/pixel at 50 km)
Field of View	2.347° × 1.173°	48° × 24°
TDI	Typically ≤18 lines of Time Delay Integration	

Radar for Europa Assessment and Sounding: Ocean to Near-surface (REASON)

Don Blankenship, University of Texas Institute for Geophysics, Austin

- Characterize the distribution of any shallow subsurface water
- Search for an ice-ocean interface and characterize the ice shell's global thermophysical structure
- Investigate the processes governing material exchange among the ocean, ice shell, surface, and atmosphere
- Constrain the amplitude and phase of the tides
- Characterize scientifically compelling sites, and hazards, for a potential future landed mission

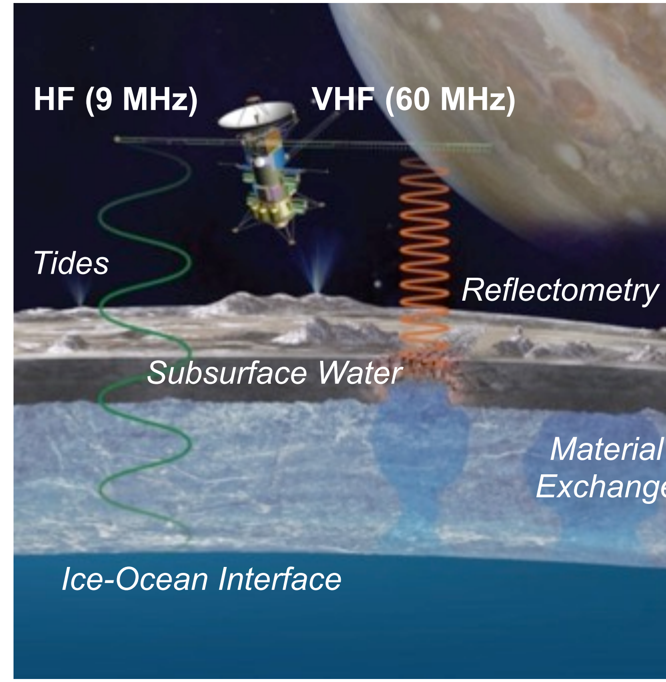

- Simultaneous high-resolution shallow sounding, altimetry, and reflectometry, along with lower resolution, full depth sounding of the ice shell and plasma measurements

Key instrument Parameters	
Dual Frequencies	60 MHz (λ = 5 m) Very High Frequency (VHF) globally, and 9 MHz (λ = 33.3 m) High Frequency (HF) anti-Jovian
Vertical Resolution	*Shallow sounding*: VHF with <15 m resolution from depths of 300 m to 3 km; *Deep sounding*: VHF or HF with <150 m resolution from depths of 1 km to 30km; *Altimetry*: VHF with <15m resolution
Antenna	2 deployable HF and 4 VHF dipole antennas mounted on solar array
Radiated Power	10-30 W

Europa Thermal Imaging System (E-THEMIS)

Philip Christensen, Arizona State University

- Detect and characterize thermal anomalies that may indicate recent activity
- Identify active plumes
- Determine the regolith particle size, block abundance and subsurface layering for surface process studies

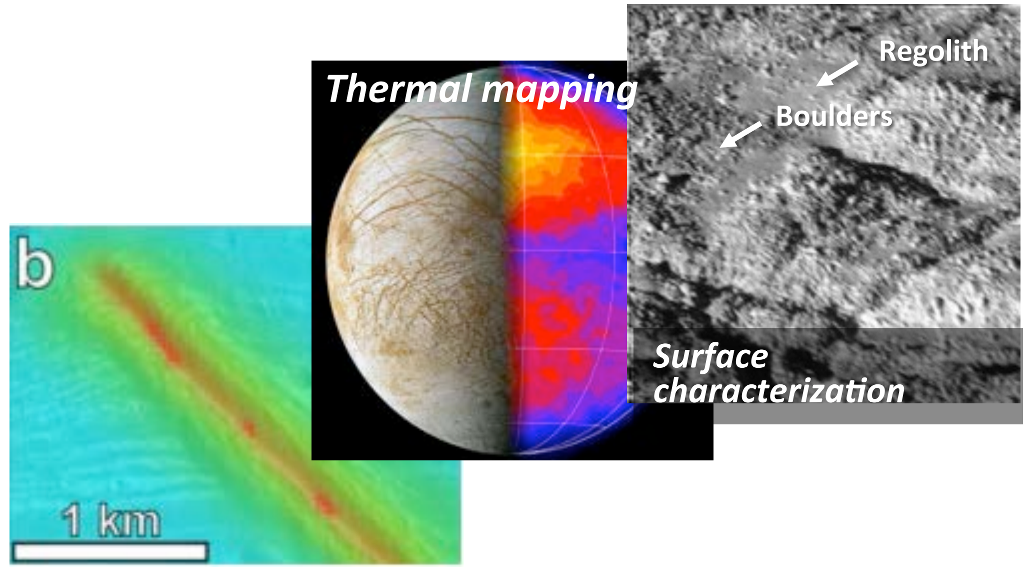

- High-resolution thermal images
- Uncooled microbolometer array with three spectral channels
- Time-delay integration (TDI) for measuring low temperatures

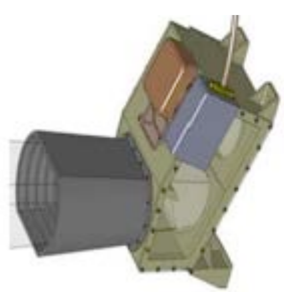

Key instrument Parameters	
Filters	7–14, 14–28, 28–70 µm
Resolution	5 – 35 m at 25 km range
Image width	5.7° cross-track (720 pixels)
Radiometric Precision	1 K for global-scale observations; 2 K for local-scale observations
Radiometric accuracy	1.25%
Time Delay Integration	16 lines

Gravity Science Investigation

Sean Solomon, Chair, Gravity Science Working Group, for Phase A

- Characterize Europa's time-varying gravitational tides (k_2)
- Confirm the existence of Europa's subsurface ocean
- In combination with radar altimetry (h_2), constrain ice shell thickness

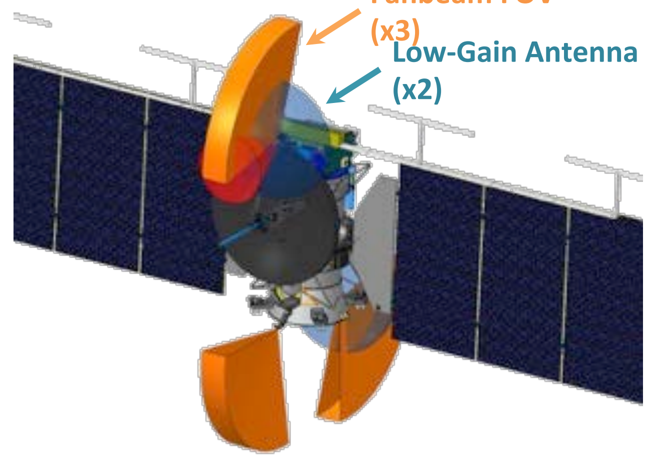

- Three Fixed Fanbeam (FB) antennas, plus utilizes two low-gain antennas (LGAs) to fill in coverage esp. for high-latitude fly-bys
- X-band up & down
- Radio Science Receivers used at DSN
- Opportunities for arraying DSN antennas and augmenting DSN with ESA antennas
- Non-intrusive with the suite of science instruments during flyby

Key Parameters	
Gain	4 - 10 dB-Hz min @D/L
Fanbeam FOV	±15˚ by ±50˚
Resolution	0.07 mm s^{-1} (60 s integration time)

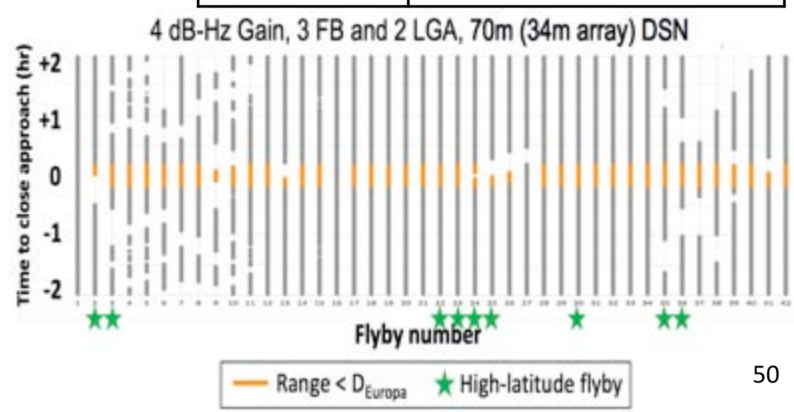

Trajectory Development (16F11)

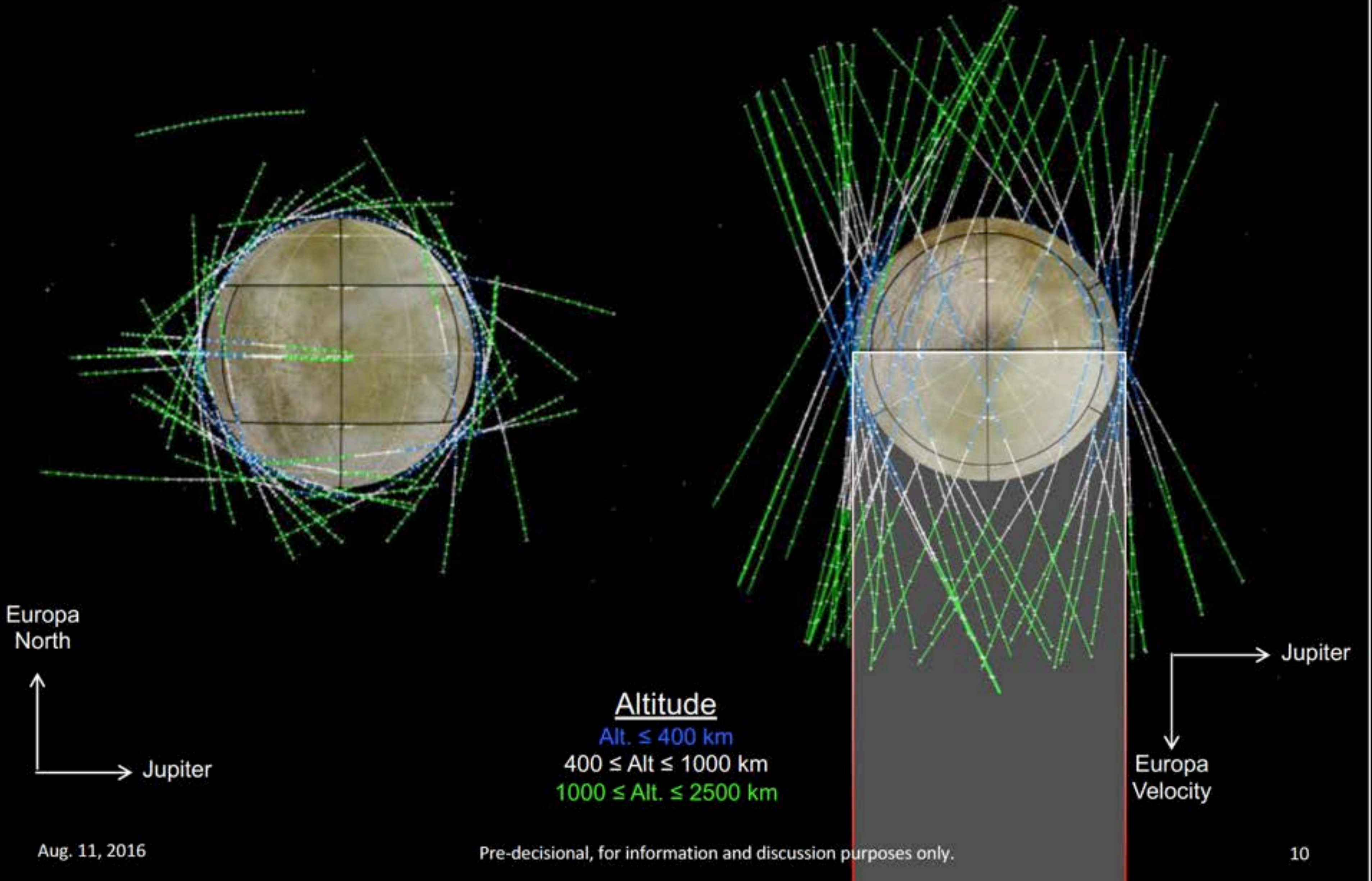

Comprehensive Surface Coverage

Ground tracks permit globally distributed regional coverage

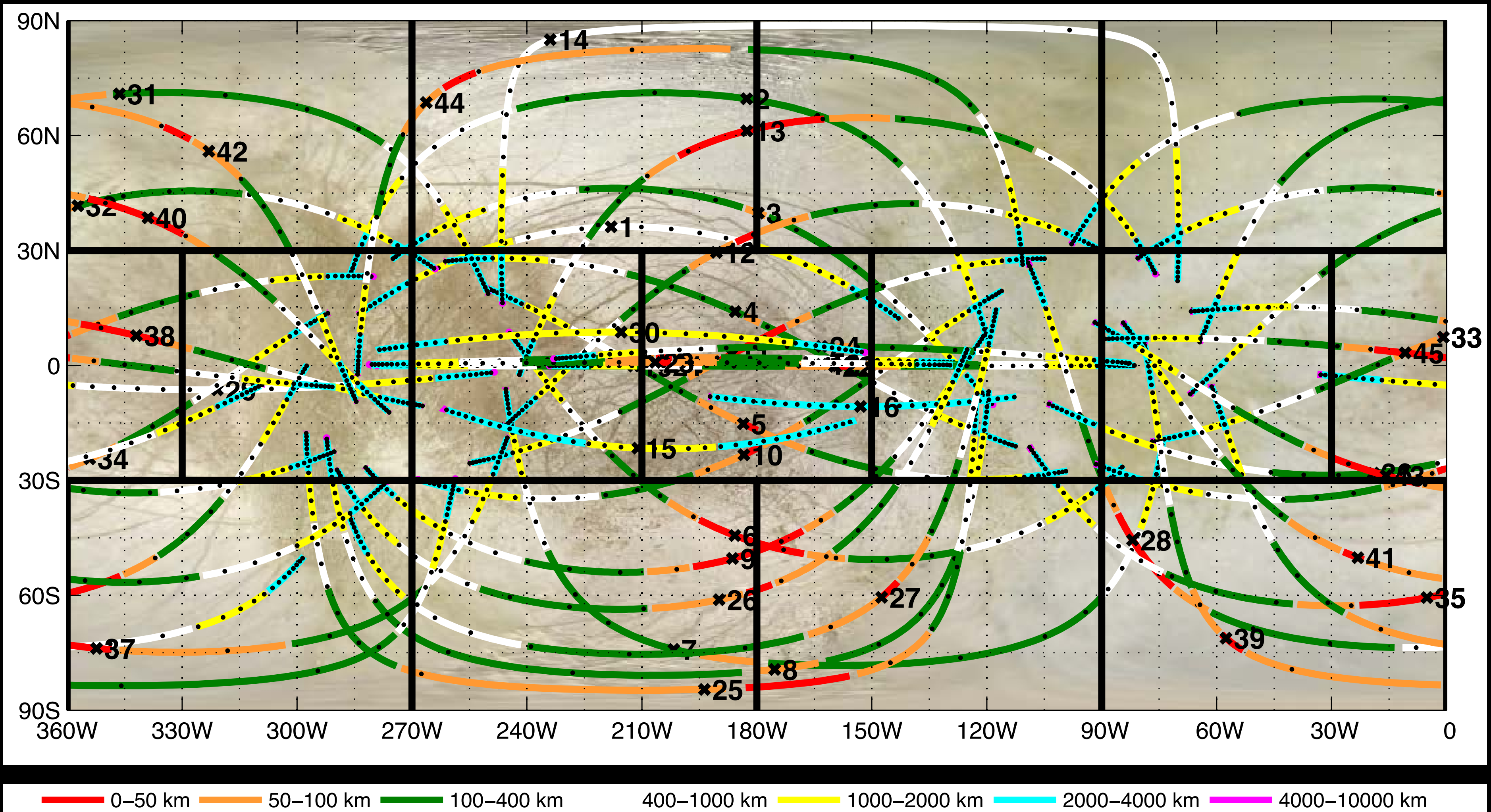

- Above 1,000 km: 2
- 250 km to 750 km: 6
- 80 km to 100 km: 9
- 50 km: 18
- 25 km: 10

Hypothetical example from the Jupiter Europa Orbiter mission study using geophysical techniques

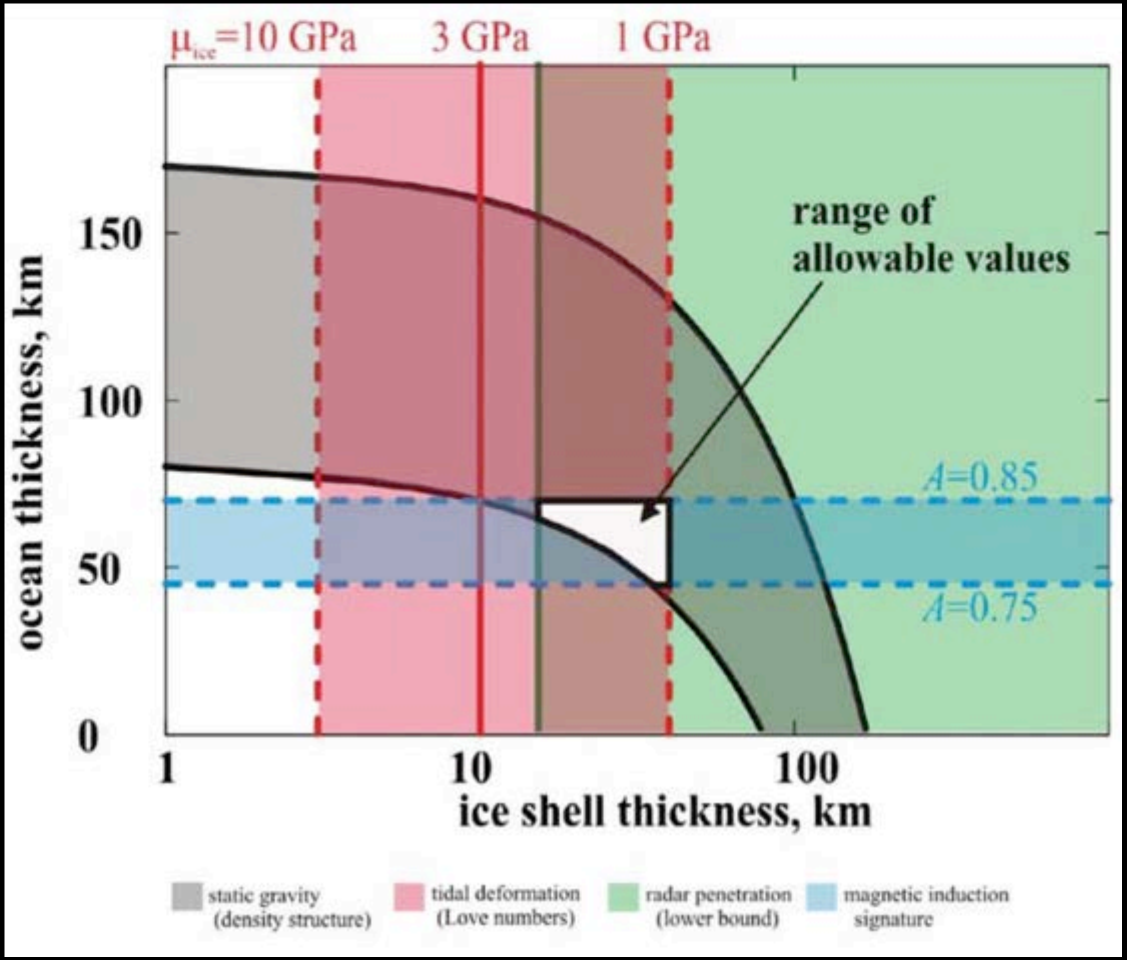

EJSM final report, 2010

Europa Lander

Comparison of Europa's surface age with terrestrial bodies

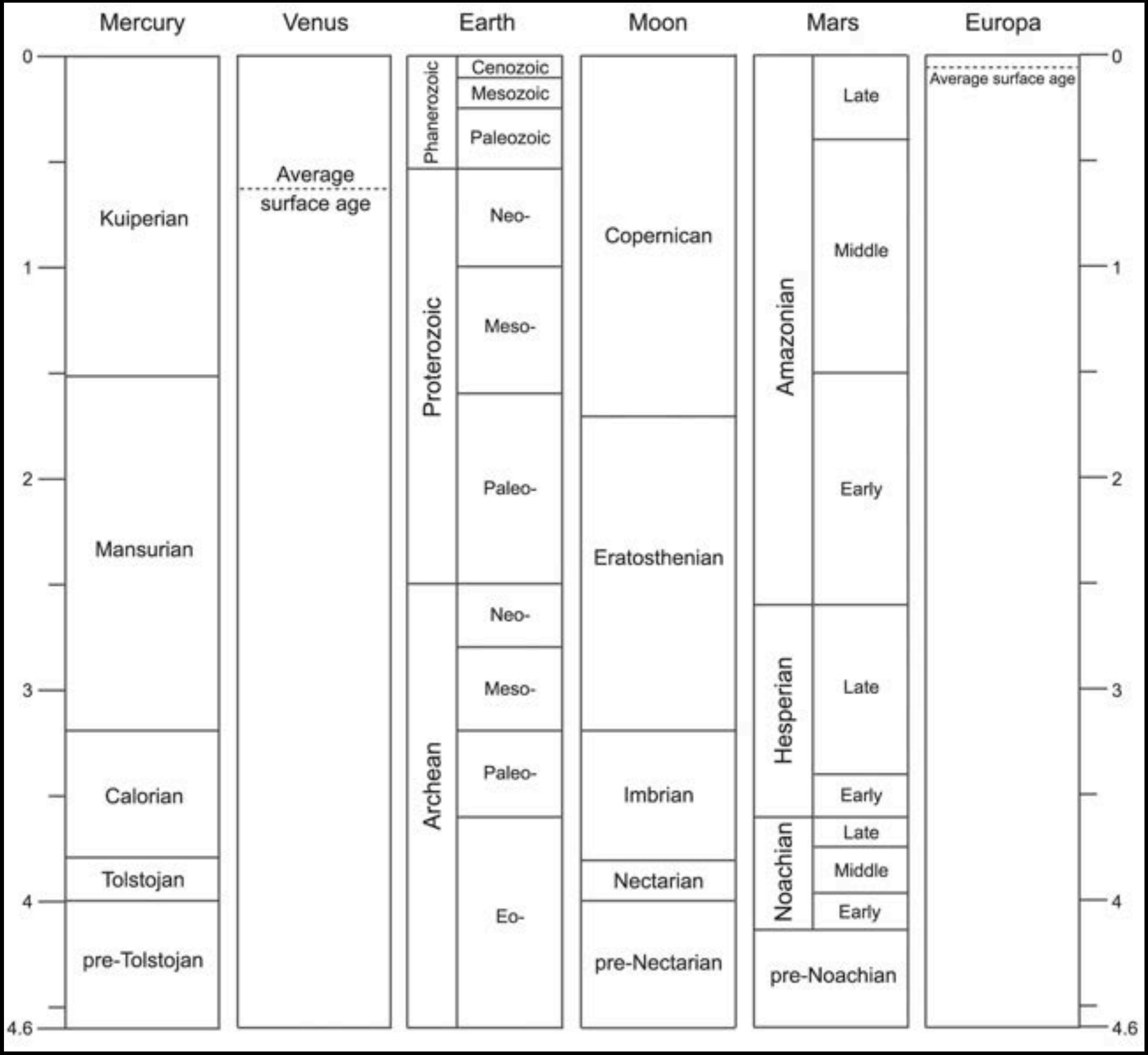

Doggett et al., 2007

Cyclical Geological Activity?

- Mapping suggests geological changes:
  - Transition from ridged plains to chaos; waning activity
- Strange for a surface just ~40–90 Myr old
- Tidal heating and orbital evolution of the 3 resonant Galilean satellites are linked:
  - Possible cyclical tidal heating & geological activity

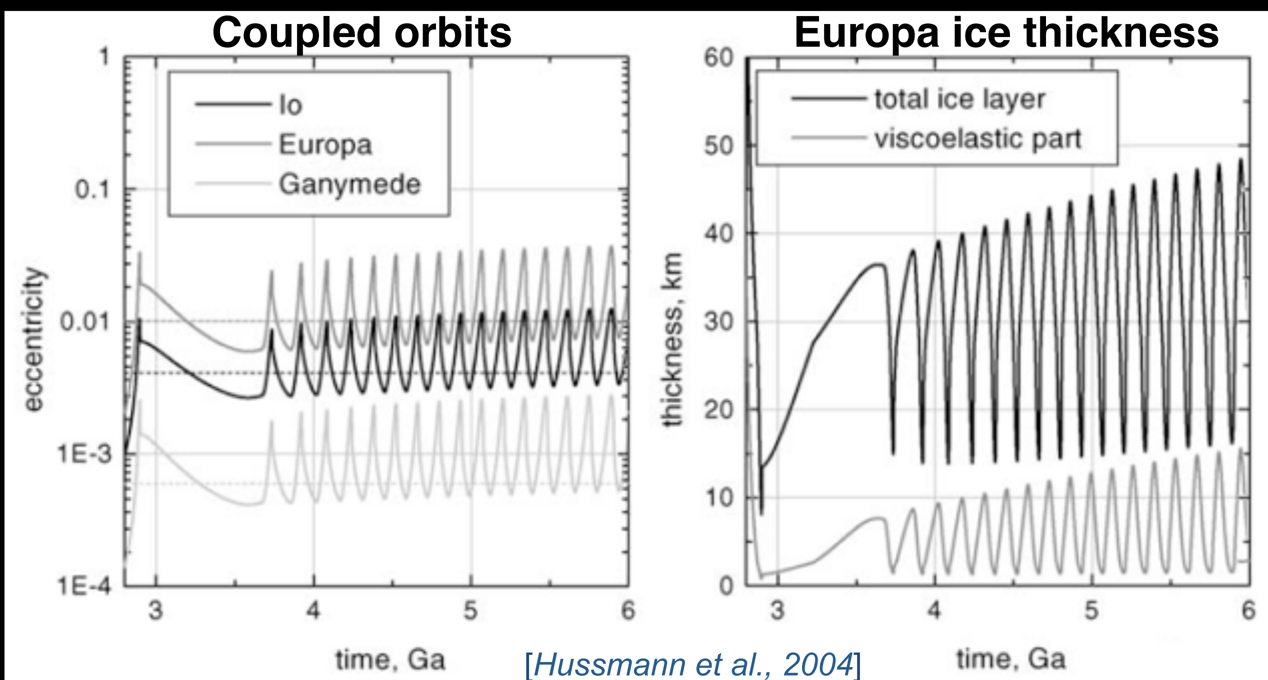

[*Hussmann et al., 2004*]

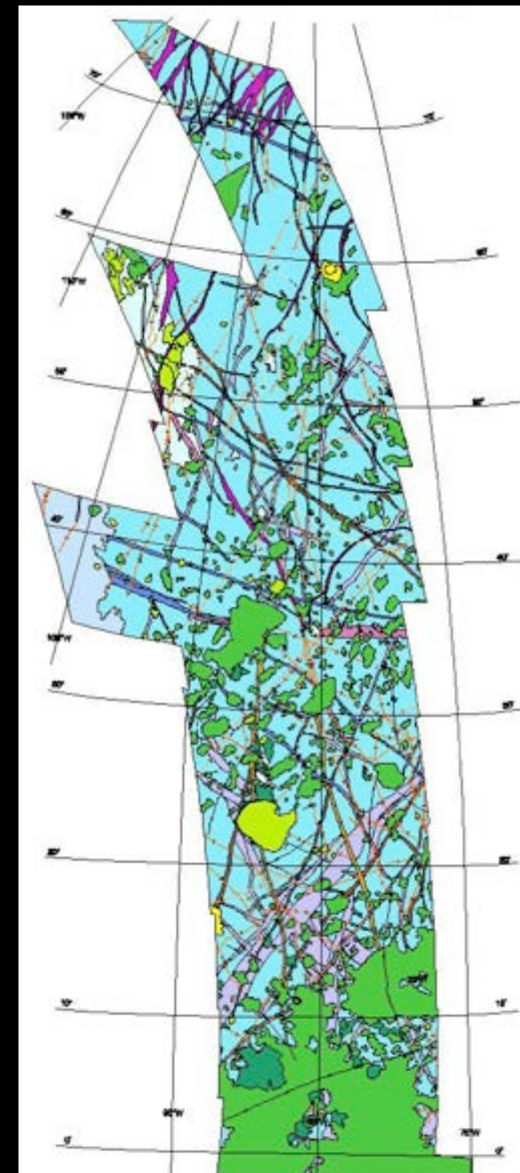

[*Figueredo & Greeley, 2004*]

How has ice shell thickness changed with time?

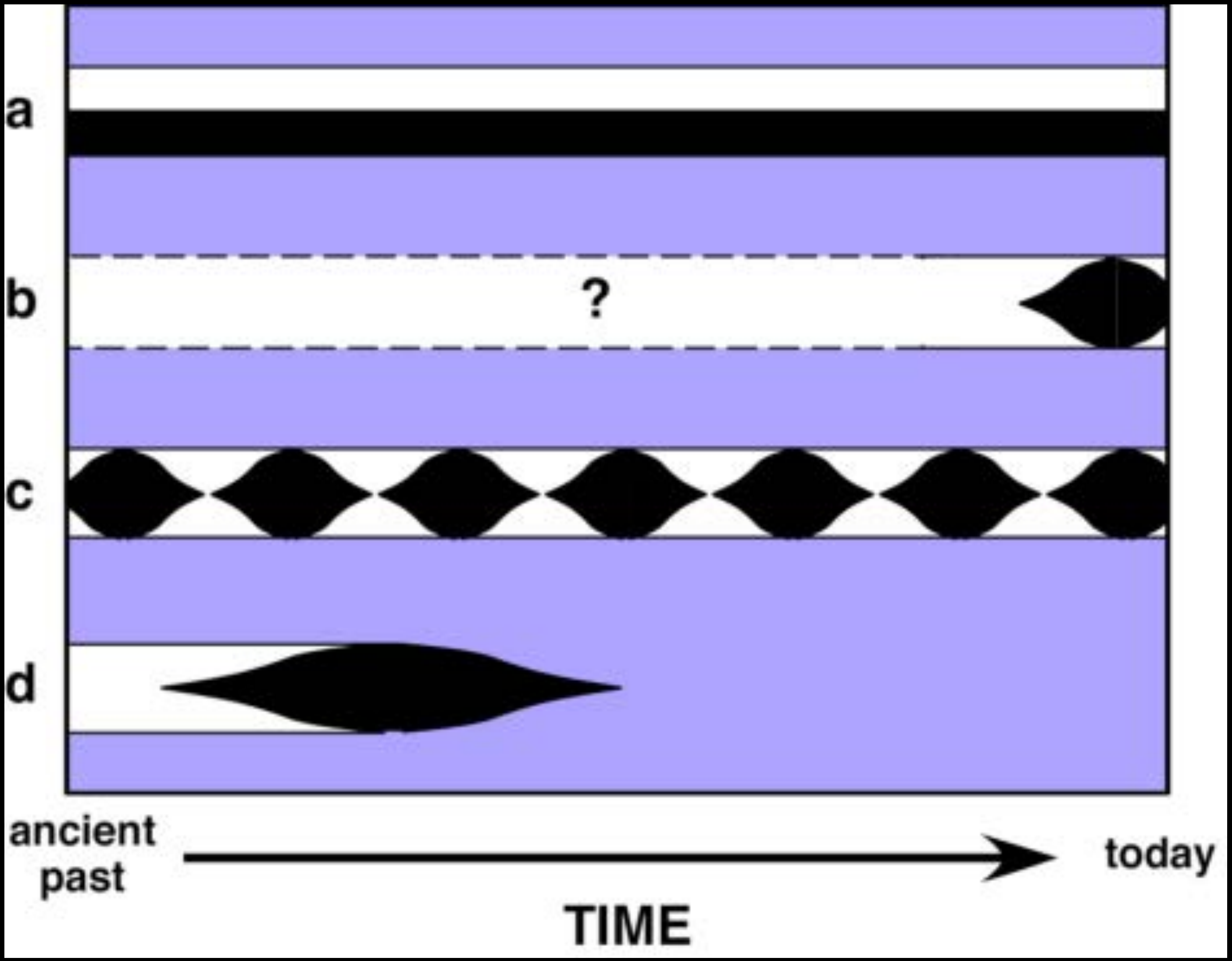

Pappalardo et al., 1999

Summary

- Multiple lines of evidence suggest that Europa’s ice shell is likely >15 km thick
- There is ample evidence for recent liquid on Europa’s surface, but such liquid may not originate directly from Europa’s ocean
- **There are probably thin portions of the ice shell; these are likely to be situated above subsurface lenses of liquid or warm ice**
- Data from the Europa Clipper mission will (and a potential future Europa Lander would) constrain the structure and thickness of Europa’s shell

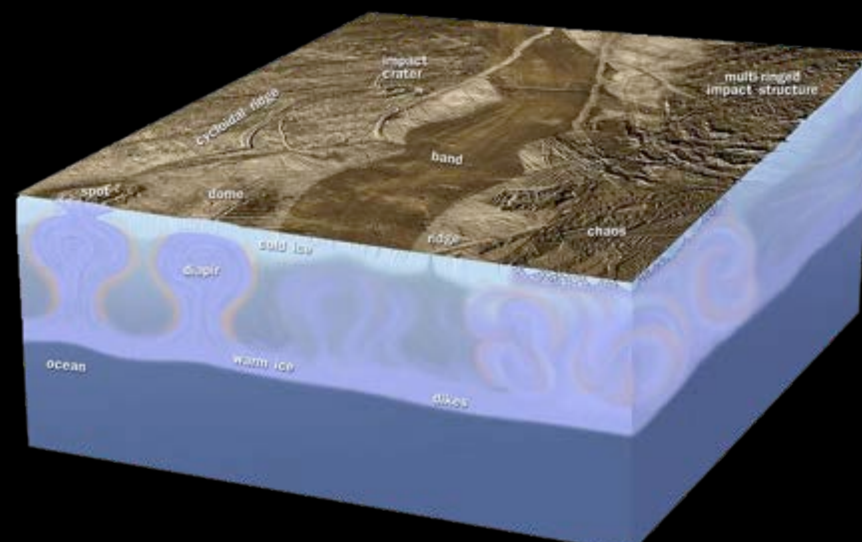

Backup

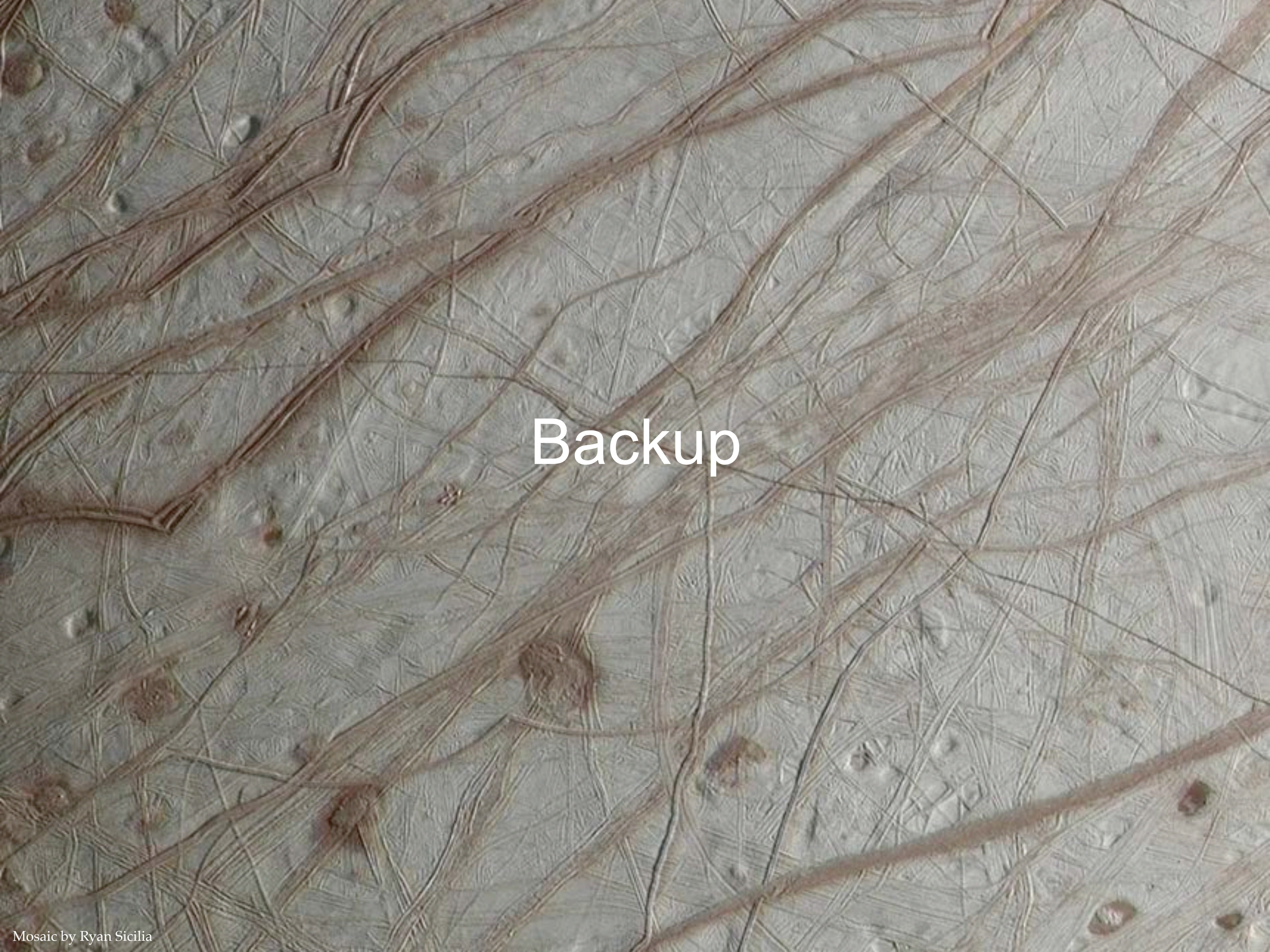

Mosaic by Ryan Sicilia

Source	Magnitude	Notes/References
Diurnal tides	<~100 kPa	*Greenberg et al.* (2002)
Librations	Comparable to diurnal?	Bills et al. (this volume); ***Sarid et al.*** (2006)
Nonsynchronous rotation	Several MPa	***McEwen*** (1986); ***Leith and McKinnon*** (1996); ***Geissler et al.*** (1998a); Sotin et al. (this volume)
Polar wander	Several MPa	*Leith and McKinnon (1996)*; ***Schenk et al.*** (2008)
Thermal convection	<100 kPa	*McKinnon* (1999); *Nimmo and Manga* (2002), *Tobie et al.* (2003); *Showman and Han* (2004)
Compositional convection	<1 MPa	*Pappalardo and Barr* (2004); *Han and Showman* (2005)
Thickening of the icy shell	Several MPa (tensile)	*Nimmo* (2004b); *Kimura et al.* (2007)
Impacts	TPa	Locally; duration ~ tens of seconds
Cycloid propagation	<40 kPa	***Hoppa et al.*** (1999a)
Normal faults	>6–8 MPa	***Nimmo and Schenk*** (2006)
Band rifting	0.3–2 MPa	***Stempel et al.*** (2005); *Nimmo* (2004d)

References in bold denote observationally constrained values.

TABLE 2. Source and magnitude of strain rates.

Source	Magnitude	Notes/References
Diurnal tides	2×10^{-10} s^{-1}	*Ojakangas and Stevenson* (1989a)
Opening of bands	10^{-15}–10^{-12} s^{-1}	*Nimmo* (2004d); ***Stempel et al.*** (2005)
Nonsynchronous rotation	<~10^{-14} s^{-1}	***Hoppa et al.*** (1999b)
Undeformed craters	<10^{-16} s^{-1}?	Assumes <10% local strain and crater age of 30 m.y.; only applies to postcratering deformation

References in bold denote observationally constrained values.

Nimmo and Manga 2007